Volume 8 | Number 10 | October 2015 | Pages 2799–3050

Energy & Environmental Science

www.rsc.org/ees

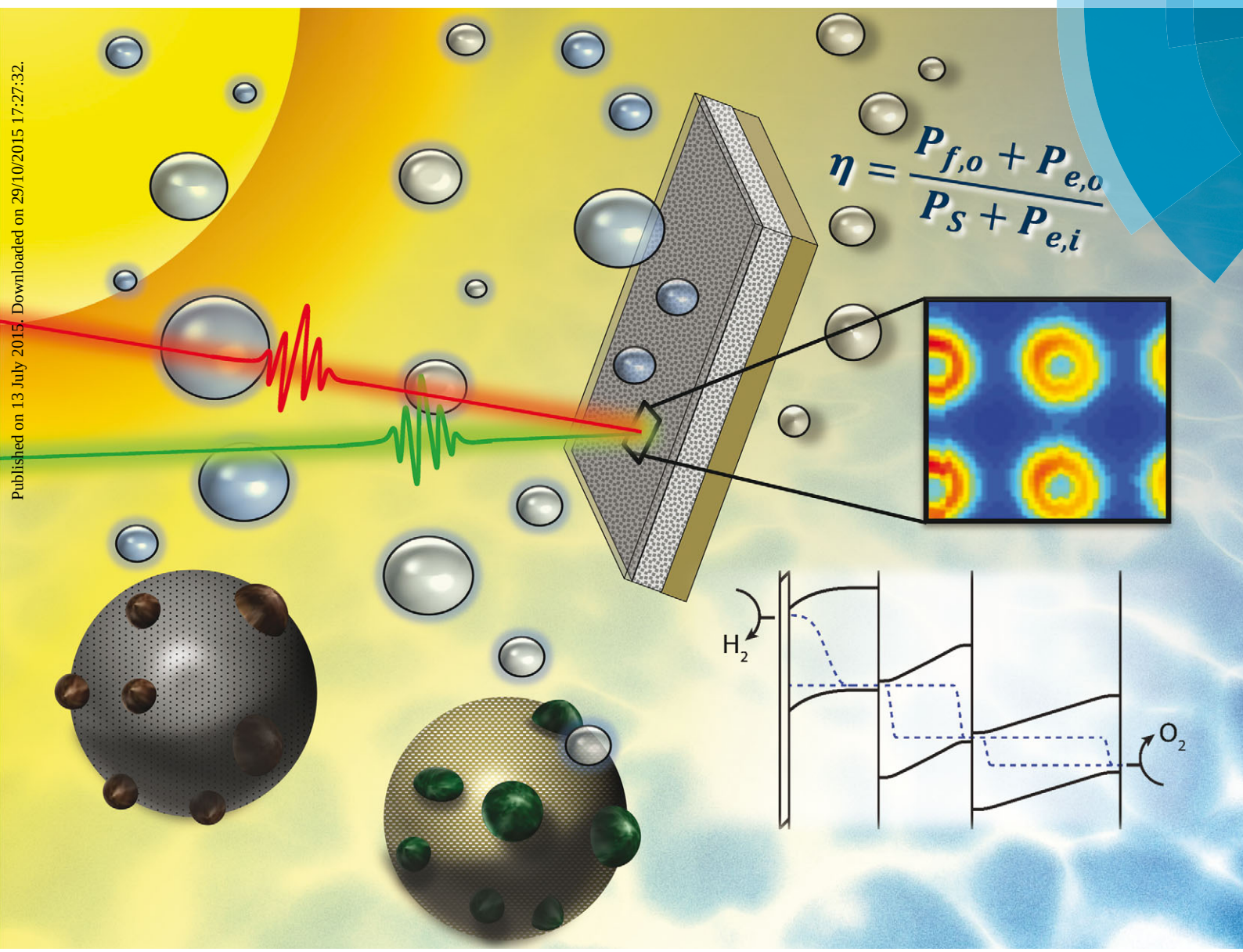

ISSN 1754-5692

ROYAL SOCIETY OF CHEMISTRY

SPECIAL COLLECTION
Editorial by Eric Miller, with contributions from Ager *et al.*, Fabian *et al.*, Coridan *et al.*, Smith *et al.* and Esposito *et al.*
Photoelectrochemical Water Splitting

Energy & Environmental Science

ROYAL SOCIETY OF CHEMISTRY

REVIEW

Cite this: *Energy Environ. Sci.*, 2015, **8**, 2825

Particle suspension reactors and materials for solar-driven water splitting

David M. Fabian,[a] Shu Hu,[b] Nirala Singh,[c] Frances A. Houle,[d] Takashi Hisatomi,[e] Kazunari Domen,[e] Frank E. Osterloh[f] and Shane Ardo*[ag]

Received 8th May 2015,
Accepted 13th July 2015

DOI: 10.1039/c5ee01434d

www.rsc.org/ees

Reactors based on particle suspensions for the capture, conversion, storage, and use of solar energy as H_2 are projected to be cost-competitive with fossil fuels. In light of this, this review paper summarizes state-of-the-art particle light absorbers and cocatalysts as suspensions (photocatalysts) that demonstrate visible-light-driven water splitting on the laboratory scale. Also presented are reactor descriptions, theoretical considerations particular to particle suspension reactors, and efficiency and performance characterization metrics. Opportunities for targeted research, analysis, and development of reactor designs are highlighted.

Broader context

Global climate disruption fueled by anthropogenic greenhouse gas emissions is a major concern for humanity and life on Earth. The only way to significantly attenuate the rate of carbon dioxide emitted into the atmosphere is to reduce fossil fuel use for energy and industrial applications. Hydrogen produced by water splitting using renewable solar energy is a clean replacement for fossil fuels. Solar photoelectrochemical water splitting represents a "Holy Grail" technology, but faces challenges before solar hydrogen can compete with fossil fuels on a cost-per-energy basis. To make solar hydrogen feasible, particle suspension reactors projected to cost less than fixed-electrode designs must be coupled with low-cost, stable, and efficient materials. Should these proposed technologies become a reality, society will have an economic impetus to use clean hydrogen as a fuel source for important industrial processes such as transportation and production of chemicals including ethylene and ammonia.

I. Introduction

Practical solar water splitting, *i.e.* $2H_2O \rightarrow 2H_2 + O_2$, using Earth-abundant materials was branded a Holy Grail of chemistry.[1] Specifically, the charge was to demonstrate >10% efficiency, >10 year stability, and a cost of hydrogen that is competitive with the cost of fossil fuels, on an energy equivalent basis. Toward this, numerous laboratory demonstrations of photoelectrochemical (PEC) water splitting have been reported. The most efficient demonstrations use a fixed-electrode design where the light-absorber materials resemble that of a solar-cell light absorber immersed into, or in the vicinity of, an aqueous electrolyte. PEC reactors for centralized H_2 production using this design have been termed Type 3 and Type 4 reactors,[2,3] where the latter is operated under conditions of concentrated solar illumination. The techno-economics of these two designs have been analyzed, and both were projected to produce hydrogen with the energy content of a gallon of gasoline for less than the price of a gallon of gasoline in the United States of America (U.S.). However, these analyses required that the reactors operate at approximately the maximum practical energy-conversion efficiency for solar-to-hydrogen evolution through water splitting (STH), *i.e.* ~25%.[2–8] Alternative reactor designs for centralized H_2 production utilize particle suspensions where the particles are free to move in their mixture with the electrolyte and are not incorporated as part of a membrane to separate sites of anodic and cathodic redox chemistry. These designs have been termed Type 1 and Type 2 reactors based on the number of different reactor vessels and were projected to be cost-competitive with gasoline sold in the U.S., on an energy basis, when operated at an STH efficiency of 5–10%, and even lower under certain circumstances. This is particularly notable in light of the laboratory-scale demonstrations that have achieved >18% STH efficiency for designs that are amenable to Type 3 reactors.[9,10]

[a] *Department of Chemistry, University of California Irvine, Irvine, CA 92697, USA. E-mail: ardo@uci.edu*
[b] *Joint Center for Artificial Photosynthesis, California Institute of Technology, Pasadena, CA 91125, USA*
[c] *Department of Chemical Engineering, University of California Santa Barbara, Santa Barbara, CA 93106, USA*
[d] *Joint Center for Artificial Photosynthesis, Lawrence Berkeley National Laboratory, Berkeley, CA 94720, USA*
[e] *Department of Chemical System Engineering, The University of Tokyo, Tokyo 113-8656, Japan*
[f] *Department of Chemistry, University of California Davis, Davis, CA 95616, USA*
[g] *Department of Chemical Engineering and Materials Science, University of California Irvine, Irvine, CA 92697, USA*

Although these techno-economic analyses required many technological and cost assumptions, the low projected cost of particle suspension reactors serves as an impetus for continued and expanded research into Type 1 and Type 2 reactor designs, and motivates this review paper.

The central focus of this review paper is solar (visible-light-driven) PEC water splitting using particle suspension reactors. There are two general designs for these reactors: Type 1, which evolves H_2 and O_2 in the same vessel; and Type 2, which evolves H_2 and O_2 in separate vessels and also generates intermediate chemical species that serve as a redox shuttle between the vessels *via* a Z-scheme mechanism (Fig. 1).[2,3] This and other terminology relevant to this review paper are summarized in Table 1. Reported laboratory-scale demonstrations are summarized below. Reactor-level engineering considerations and particle characterization methods are also presented as well as various opportunities for continued research, analysis, and development that would further the understanding of these complex designs and identify potential routes for advancement of particle suspension technologies for solar PEC water splitting.

II. Reactors

By definition, particle suspensions allow complete intermixing of at least two of the oxidation and reduction chemical products in a single electrolyte, which together contain stored electrochemical potential. This is because both oxidation and reduction

David M. Fabian

David Fabian is a second-year graduate student in the Department of Chemistry at the University of California, Irvine under the supervision of Prof. Shane Ardo. He received his bachelor's degree in chemistry from The College of William & Mary in 2013 and is a 2014 NSF Graduate Research Fellow. His major research interest covers synthesis and characterization of hybrid organic–inorganic materials for applications in solution-processed thin-film photovoltaics.

Shu Hu

Shu Hu is a senior postdoctoral scholar at the Joint Center for Artificial Photosynthesis. He received his BEng (Honors) from Tsinghua University in 2006 and completed a PhD in Materials Science at Stanford University in 2011. Shu then joined the group of Prof. Nathan S. Lewis in the Division of Chemistry and Chemical Engineering at the California Institute of Technology, where his work spans experimental and modeling areas in Si and III–V nanocrystal synthesis, nanophotonic phenomena, and solid–electrolyte interfaces for photoelectrochemical solar-fuel production. His main thrust includes the stabilization of technologically important, efficient yet unstable semiconductors under photoanodic conditions relevant to water oxidation.

Nirala Singh

Nirala Singh received his PhD in 2015 from the University of California at Santa Barbara (UCSB). At UCSB he researched catalysts for the efficient production of hydrogen from sources such as hydrogen bromide, technoeconomics of renewable energy production, and photoelectrochemical absorbers for fuel and chemical production. His previous works include developing a Solar Energy Course and Lab Equipment at the University of Michigan, electrolysis of water for hydrogen production and bacteria decomposition for water purification, and testing and characterization of high-power semiconductor devices. His interests include the use of catalysis for energy production and storage.

Frances A. Houle

Frances Houle is Department Head for the Science of Large Scale Systems in the Joint Center for Artificial Photosynthesis, and Senior Scientist in the Chemical Sciences Division at Lawrence Berkeley National Laboratory. Her scientific interests are in the areas of nanoscale mechanisms of surfaces and thin-film chemical transformations. She received a BA from the University of California Irvine and a PhD from the California Institute of Technology, both in chemistry. Prior to joining LBNL she was Research Staff Member in the IBM Research Division in San Jose, California, and Manager of Materials Development at InVisage Technologies, a startup company making nanoparticle-based image sensors.

half-reactions occur on each light-absorber particle (or particles, if multiple particles are in solid-state contact). In the Type 1 reactor design the only required products of the chemical reactions are H_2 and O_2, and H^+ or OH^- which are assumed to rapidly equilibrate *via* mass transfer around each particle. Each particle (or particles, if multiple are in solid-state contact) drives both the hydrogen evolution reaction (HER) and the oxygen evolution reaction (OER) (Fig. 2a).[12] A drawback of this design is that an explosive mixture of H_2 and O_2 is evolved in one vessel.

The Type 2 reactor design does not present an explosive hazard but does introduce additional redox-active molecules. The desired products of the chemical reactions are H_2, O_2, H^+ or OH^-, and at least two redox states of a reversible (molecular) redox shuttle. H_2, the redox shuttle in a higher oxidation state, and OH^- (or water *via* deprotonation of H_3O^+) are generated by particles in one vessel, while O_2, the redox shuttle in a lower oxidation state, and H^+ (or water *via* protonation of OH^-) are generated by particles in a second vessel (Fig. 2b). In order to neutralize pH differences, protons or hydroxide ions that are generated and consumed by the HER and the OER must be transported large distances between the vessels. Alternatively, redox shuttles that undergo proton-coupled electron-transfer reactions can be used where large pH differences are not formed because small changes in pH are neutralized at each particle. Electronic charge must also be transferred between the two vessels, which can occur by several means. The redox shuttle can carry electrons by mass transport (convection and diffusion), while dragging along counterions due to local electric fields (Fig. 1c).

Takashi Hisatomi

Takashi Hisatomi received his PhD in Engineering from the University of Tokyo under Prof. Dr Domen's supervision in March 2010. He joined Laboratory of Photonics and Interfaces in École Polytechnique Fédérale de Lausanne led by Prof. Dr Grätzel in April 2010 as a postdoctoral fellow. He has been studying in Prof. Dr Domen's laboratory in the University of Tokyo since April 2012 and works as an assistant professor currently. His major research interest covers material development and device design for photocatalytic and photoelectrochemical solar water splitting as well as kinetic assessments of photocatalysis and photoelectrochemistry.

Kazunari Domen

Prof. Kazunari Domen received BSc (1976), MSc (1979), and PhD (1982) honors in chemistry from the University of Tokyo. Dr Domen joined Chemical Resources Laboratory, Tokyo Institute of Technology, in 1982 as Assistant Professor and was promoted to Associate Professor in 1990 and Professor in 1996, having moved to the University of Tokyo as Professor in 2004. Prof. Domen has been working on the overall water splitting reaction on heterogeneous photocatalysts to generate clean and recyclable hydrogen. His research interest now includes heterogeneous catalysis and materials chemistry, with particular focus on surface chemical reaction dynamics, photocatalysis, solid-acid catalysis, and mesoporous materials.

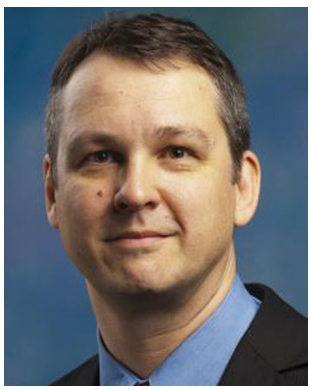

Frank E. Osterloh

Frank Osterloh is an inorganic chemist working on nanoparticle devices for artificial photosynthesis. He received MA and PhD degrees in chemistry in 1994 and 1997 from the Carl von Ossietzky University in Oldenburg, Germany, while working with late Prof. Siegfried Pohl. After completing postdoctoral training with Prof. Richard H. Holm at Harvard University, he joined the faculty at the Chemistry Department at the University of California, Davis in 2000. Since then, Frank has authored four review articles and over 75 experimental papers. In 2010, his contributions to the chemistry of nanoparticles were recognized with the ACS Inorganic Nanoscience award.

Shane Ardo

Shane Ardo is an Assistant Professor at the University of California, Irvine in the Department of Chemistry, with a joint appointment in the Department of Chemical Engineering and Materials Science. He obtained a BS in mathematics from Towson University in 1999, an MS in nutrition and food science from UM-College Park in 2005, and a PhD in photo-physical inorganic chemistry from Johns Hopkins University under Prof. Gerald Meyer in 2010. After a postdoctoral appointment at the California Institute of Technology under Prof. Nathan Lewis, he joined the faculty at the University of California, Irvine in 2013. Prof. Ardo's research interests are driven by the pursuit of understanding and controlling energy conversion mechanisms for applications in solar fuels devices, photovoltaics, seawater desalination, and redox flow batteries.

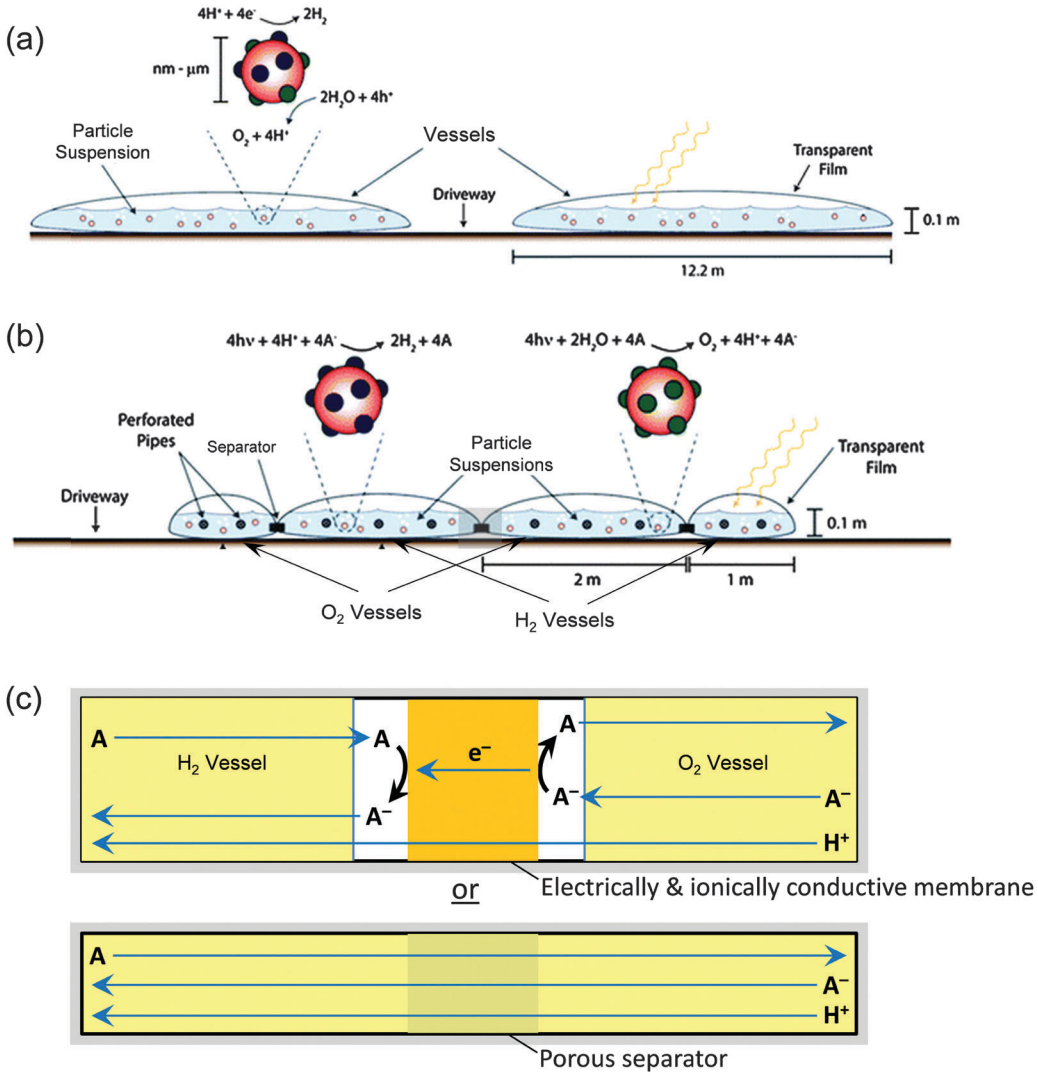

Fig. 1 Two general designs for (a) a Type 1 reactor and (b) a Type 2 reactor, where in the Type 2 reactor the separator consists of (c) a nanoporous material or an electrically and ionically conductive material(s). Yellow areas in panel (c) indicate regions where diffusion and/or convection of the redox shuttle, A/A^-, are the dominant transport mechanisms, while the white areas depict regions of redox reactivity and the orange area depicts a region of electron conduction and ion migration.[2,3] Images in panels (a) and (b) adapted from ref. 3 with permission from the Royal Society of Chemistry.

Alternatively, electrically conductive materials (*e.g.* a wire) with low overpotential for redox shuttle electrocatalysis can transport electrons at a much faster rate and is limited only by the resistance of counterion drift in the liquid electrolyte and through the ion-exchange membrane separator (Fig. 1c).[13] An additional advantage of this "wired" design is that redox shuttles in different vessels do not mix and thus a redox shuttle that is best suited for the PEC reactions in each vessel can be used.

(A) Vessel material

A prior sensitivity analysis of both reactor designs suggested that the gravimetric levelized cost of H_2 at the plant gate would be most influenced by the cost of the vessel material, *i.e.* the plastic.[14] The aforementioned techno-economic analysis proposed that the predominant vessel material be high-density polyethylene (HDPE) in part because it is an inexpensive, mass-produced plastic.[15] HDPE has been used in similar baggie-type reactors, such as those for photo-biological H_2 production from algae, and has exhibited long-term stability under solar irradiation.[2,3,16] HDPE is chemically stable over the entire pH range (0–14) and is thermally stable to at least 60 °C,[17] the approximate maximum temperature that a solar PEC water-splitting reactor will likely reach. Also, H_2 permeability in HDPE is low,[18] and a reasonable thickness can be chosen ($\sim$0.5 cm) that results in transmission of $\sim$90% of the incident solar illumination with only a $<$1% loss of evolved H_2.[19] Thus, HDPE and similar optically transparent, robust, and inexpensive plastics are likely good candidate materials for the reactor vessels.

(B) Challenges for Type 1 reactors

A major practical technical challenge with the Type 1 reactor is the need to separate the explosive mixture of H_2 and O_2 gases in

Table 1 Device terminology

Photoelectrochemical (PEC) water splitting	Light-driven water electrolysis into only H_2 and O_2
Suspension	A mixture or slurry solution of non-fixed solid electrode particles, which when completely dispersed and suspended in another substance on the sub-micron scale are termed colloidal
Tandem particles	Two light-absorber particles that are connected electrically in series *via* a solid-state contact or *via* a redox shuttle
Redox shuttle	An electrolyte additive that is redox active and mediates charge transport between two locations
Type 1 reactor	A single-vessel reactor that evolves H_2 and O_2 in the same space
Type 2 reactor	A reactor that evolves H_2 and O_2 in separate vessels and thus requires a solution redox shuttle to facilitate the transfer of electrons and ions between the vessels
Z-scheme	A PEC mechanism that utilizes tandem particles and is suitable for use in a Type 1 or Type 2 reactor
HER	Hydrogen-evolution reaction, which electrochemically converts H_2O or H^+ into H_2 *via* electron-transfer reactions
OER	Oxygen-evolution reaction, which electrochemically converts H_2O or OH^- into O_2 *via* electron-transfer reactions
Cocatalyst	An electrocatalyst that is incorporated with another material to improve the rate of a faradaic reaction
STH efficiency	Solar-to-hydrogen energy-conversion efficiency for converting the energy in incident solar irradiation to chemical bonds as H_2 through oxidation of water to O_2
QY	Quantum yield, which is the ratio of the number of output events that occur per number of input stimuli, which is typically the number of absorbed photons[11]
EQY	External quantum yield, which for suspensions is often termed the apparent QY and should be defined as the ratio of two times the rate of collection of H_2 (mol H_2 cm^{-2} s^{-1}) to the incident photon flux (mol photon cm^{-2} s^{-1})
Overpotential	Potential difference between the equilibrium potential for a half-reaction and the experimentally applied bias potential at a specified current density
AM 1.5G	Air Mass 1.5 Global tilt, which is the standard spectral composition of sunlight

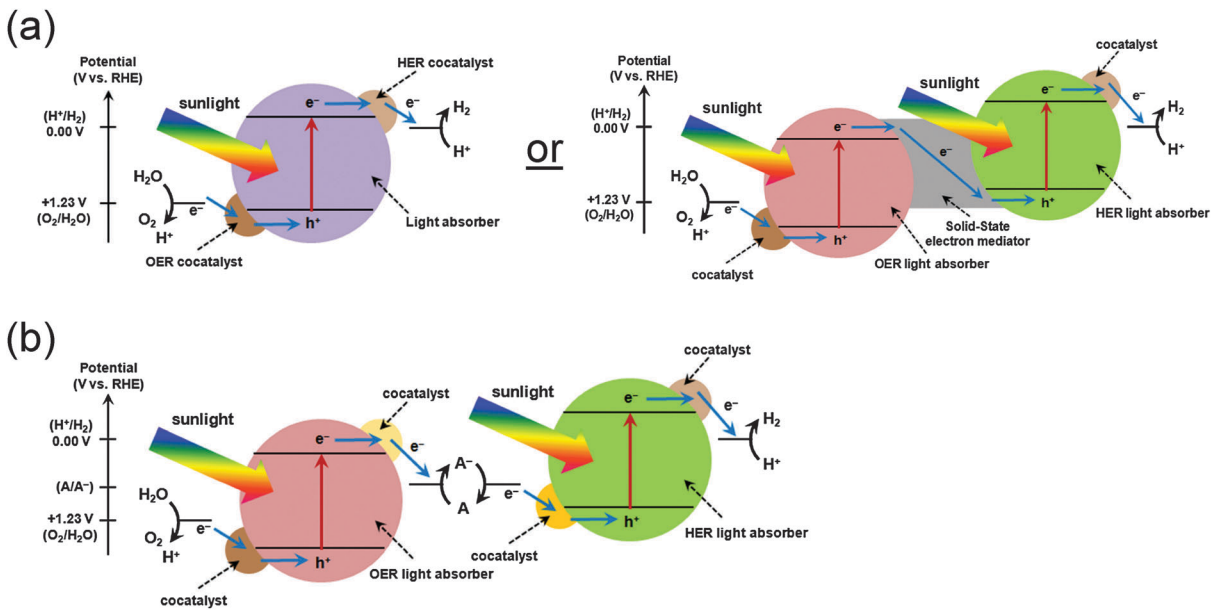

Fig. 2 Schematic of materials components, arrangements, and energetics for particles that are suitable for (a) a Type 1 reactor and (b) a Type 2 or Type 1 reactor. Adapted with permission from K. Maeda, K. Domen, *J. Phys. Chem. Lett.*, 2010, **1**, 2655–2661.[12] Copyright 2010 American Chemical Society.

the headspace of the single vessel. Preventing a flammable mixture by separating 98% of the H_2 from the evolved mixture of H_2 and O_2 so that it is below the flammability limit of 4 at% H_2 and 96 at% O_2[20] requires an estimated energy expense equal to 8.7% of the energy stored in the fuel mixture (see Appendix). In practice, the energy expense will be higher, due to the need

to power the compressor and to probably include pressure-swing-adsorption components. Gas separation is projected to constitute the largest fraction of the reactor capital costs for Type 1 reactors.[2,3] Another means to separate the H_2/O_2 product gases is through the use of a carrier gas that dilutes the H_2 and O_2 to beyond their flammability limits.[14] The carrier gas can be an inert gas, such as N_2 or Ar, or the reactor product gases, *i.e.* H_2 or O_2. Dilution with H_2 makes sense if a small concentration of O_2 (and water) in H_2 is easier to remove than a small concentration of H_2 in O_2. Moreover, this latter composition will form a combustible mixture during the concentration process if O_2 is removed from the mixture. For H_2 dilution, the original 2 : 1 v/v stoichiometric H_2/O_2 reaction product mixture (66.7 at%, 33.3 at%) would be concentrated to beyond the flammability limit of ~95 at% H_2 and ~5 at% O_2 with at least 17 parts of pure H_2 per 2 parts product H_2 and 1 part product O_2, which results in a 20/3 (6.67) volume dilution factor.[14] The energy required for the repeated H_2 separation and subsequent use as diluent followed by re-separation is projected to use >60% of the energy stored as H_2, resulting in a >60% increase in the capital costs of the gas processing subassembly, assuming a $0.10 per kW h cost of electricity.[14] These monetary and energy costs were projected to increase the levelized cost of H_2 for a Type 1 reactor by >90%.[14] This suggests that there is a strong need to design alternative gas separation and management schemes.

(C) Challenges for Type 2 reactors

A major practical technical challenge with the Type 2 reactor is that without proper electrolyte flow, the redox shuttle will not move between the vessels rapidly enough to keep concentration gradients, and thus energy losses, to a minimum. Macroscopic mass transfer of the redox shuttle is governed by the Nernst–Planck equation which states that mass transfer occurs due to a combination of diffusive flux due to Brownian motion, convective flux due to mixing, and migration flux due to the effect of electric fields on charged particles.[21,22] Mass transport of redox shuttles in particle suspension reactors will occur across and between vessels mostly by convection and diffusion. Ionic migration of counterions will occur over a short distance between the sites for each half-reaction on individual particles and near charged redox shuttles as they transport across and between vessels. Because these mass-transport processes are decoupled from the light-driven reactions, their rates can differ from the absorbed photon flux but must result in a steady-state concentration profile over day–night cycles and on the timescale of days. Per the Nernst equation, every order-of-magnitude change in redox shuttle concentration from the initial conditions results in an additional thermodynamic potential requirement of $(2.303RT/nF)$ = (59.2 mV/n) beyond that required for water splitting. Thus, slow redox-shuttle mass transport over large distances can result in significant additional thermodynamic potential requirements and concentration overpotentials. Passive diffusion between vessels described in the techno-economic analysis will not reach a steady-state redox shuttle concentration gradient, because the vessels were modeled to be on the meters length-scale. Thus, in the absence of convection the original redox state of the redox shuttle will eventually become fully depleted during solar illumination and the device will cease to operate. Moreover, the largest fraction of the reactor capital costs in a Type 2 reactor are projected to be the piping and control system subassemblies to mix the electrolytes, notably the pipes and pumps.[2,3] For these reasons, flow in Type 2 reactors is a very important design consideration.

The separator is also a key component. It must be highly impermeable and electrically insulating with respect to recombination of the reaction products, *i.e.* H_2 and O_2. Many state-of-the-art separators have been developed for other electrochemical technologies and have decades of proven industrial success. However, some are not practical for use in particle suspension reactors for solar PEC water splitting. In particular, porous materials cannot sustain pressure differentials and thus even small pressure differentials between the vessels will result in forced convection of the electrolyte across the separator.[23] For example, a ~10 mA cm^{-2} crossover current is insignificant for major industrial technologies that operate at current densities on the order of A cm^{-2}. However, because crossover currents are approximately independent of the rate of product formation and most solar PEC water-splitting devices are projected to operate at rates comparable to this crossover current density, a majority of the reaction products will mix between the vessels before they can be collected.[24] Nafion, a polytetrafluoroethylene copolymer containing perfluorinated vinyl ethers and terminal sulfonate ionic functional groups, overcomes this issue because it can withstand large pressure differentials, exhibits a low rate of crossover for H_2 and O_2, and is extremely chemically robust.[25] The latter property is important because undesired side-reactions of electrocatalysis often generate highly reactive oxygen species which will degrade most polymers. For these reasons, Nafion is the state-of-the-art ion-exchange membrane used in most fuel cells, electrolyzers, chloralkali plants, and redox-flow batteries, but represents a large fraction of the cost of these electrochemical technologies.[26] In particle suspension reactors, highly reactive hydroxyl radicals and hydrogen peroxide generated at the particles as undesired side-products of water splitting may be quenched before they can interact with the separator. This is because most of the particles are located far from the separator and although hydrogen peroxide is rather stable in aqueous solution, it rapidly disproportionates at many metal surfaces such as those often used as cocatalysts.[27] Thus, a less chemically robust and therefore less expensive membrane than Nafion may be suitable in most particle suspension reactors for solar PEC water splitting.

(D) Commercial interest

Two companies have actively pursued research and development of laboratory-scale particle suspension reactors. HyperSolar, involving Prof. Eric McFarland (University of California, Santa Barbara), fabricates and evaluates rod-shaped particles affixed in insulating alumina pores for light-driven water splitting and HBr splitting into H_2 and Br_2. Sun Catalytix, founded by Prof. Dan Nocera (Harvard University), previously investigated the techno-economics of particle suspension reactors and fabricated small-scale models.

III. Theoretical considerations

Theoretically, there are many fundamental considerations for particle suspension reactors for solar PEC water splitting that have not been thoroughly evaluated. Many of these are described below and organized by general theme. There is a great need for not only experimental analyses of the following hypotheses, but also numerical modeling and simulations ranging from the nano-scale to the device and reactor scale. As materials are developed that may be promising for application in particle suspension reactors for solar PEC water splitting, logical particle-scale and reactor-scale designs will become increasingly important and can be most effectively assessed once the considerations outlined below are clarified.

(A) Particle concentration

Without varying the size of the particles, the optical absorption of particle suspensions can be adjusted by changing the particle concentration (c_{part}) and/or vessel height (h_{vessel}) (Fig. 3a). Absorption of nearly all incident above-bandgap sunlight is possible with appropriate choice of h_{vessel} and c_{part}. Thus, the volume of the electrolyte used in a particle suspension reactor dictates the amount of light-absorber material, while in fixed-electrode designs this is not the case for the electrolyte dimension orthogonal to the face of the electrode, *i.e.* the thickness of the electrolyte toward the Sun. Engineering considerations for forced convection (*e.g.* electrolyte flow and mixing) will depend on the size of the reactor. This will dictate an optimal concentration of particles for sufficient sunlight absorption and maximum STH efficiency, which may in turn redefine the necessary amount of forced convection. The complex interdependence of particle concentration, light absorption, solvent volume, and mass transfer of reagents may require iterative reactor design engineering, which would benefit from initial assessment *in silico*.

(B) Particle size: nano-scale *vs.* micron-scale

Particle size affects the mechanisms by which light interacts with the particles and photo-excited charge carriers are separated and collected, and thus affects the STH efficiency of the reactor. Nano-scale particles present a shorter distance for collection of minority charge carriers, but require p–i–n doping distributions in order to support a space-charge region and assist in charge separation.[28–31] Two other review papers published in this journal issue by Ager *et al.* and Smith *et al.* describe the effects of semiconductor–liquid junctions *versus* buried junctions so this will not be discussed further here, except that fabrication of buried junctions is inherently a more complex and costly process but often results in increased device efficiencies and stabilities.[10,32] Moreover, in comparison to smooth micron-sized particles, smooth nanoparticles present more surface area per particle volume which lessens cocatalyst requirements. However, micron-sized particles absorb more light, because the optical path length depends on particle size and micron-sized particles also more effectively scatter light likely increasing the number of times light passes through each particle. Larger particles are also more likely to more fully support space-charge regions (Fig. 4), which often results in more efficient charge separation and larger open-circuit photovoltages,

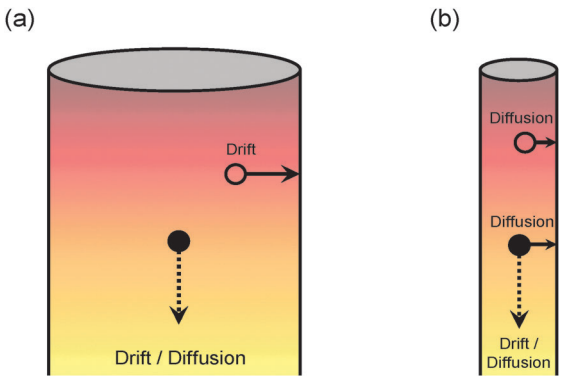

Fig. 4 Comparison of the mechanisms by which minority (open circles) and majority (filled circles) charge carriers separate in (a) thick and (b) thin high-aspect-ratio semiconductors containing the same dopant density and in contact with a redox couple that upon equilibration drives the semiconductor into inversion. The structure in (a) can support most of the space-charge region and so the concentration of majority carriers in the bulk does not change upon equilibration. Adapted with permission from A. Fitch, N. C. Strandwitz, B. S. Brunschwig, N. S. Lewis, *J. Phys. Chem. C*, 2013, **117**, 2008–2015.[35] Copyright 2013 American Chemical Society.

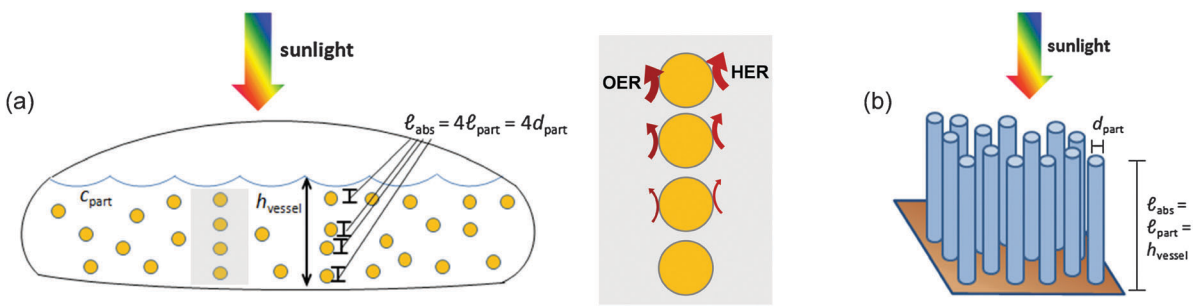

Fig. 3 Comparison between (a) a particle suspension reactor design and (b) a fixed-electrode reactor design. (a) For particle suspension reactors, vessel height (h_{vessel}) and particle concentration (c_{part}) are the most important parameters to determine an optical path length that results in significant above-bandgap sunlight absorption (ℓ_{abs}). Inset: Particles near the bottom of the vessel absorb less light and thus drive the HER and the OER at slower rates than particles near the top of the vessel, depicted by the sizes of the curved arrows. (b) The fixed-electrode design with high aspect ratio semiconductors affords rapid charge collection along the short dimension of the rods/wires (d_{part}) and maximum absorption of sunlight along the long dimension (ℓ_{part}).

assuming there are two locations for charge collection, one ohmic and the other rectifying.[33–35] For example, micron-sized particles of optimally doped silicon are required to support a near-maximum-sized space-charge region;[36] for optimally doped GaAs particles sub-micron diameters suffice.[37] In summary, key challenges for nano-scale and micron-scale particles for solar PEC water splitting are to develop optimally doped light-absorber materials with large thicknesses, to absorb a significant amount of incident above-bandgap irradiation (*e.g.* >90%), and large cocatalyst surface areas, to minimize electrocatalytic losses. A balance in the size of the minimum dimension must be attained so that it is large enough to support a space-charge region, and assist in excited-state charge separation, while also small enough to afford rapid charge collection.

(C) Particle shape: symmetric *vs.* asymmetric

Particles with highly anisotropic size and shape are generally advantageous for fixed-electrode designs. Maximum absorption of sunlight occurs when the long dimension of the particle is nearly collinear with the direction of propagation of solar photons.[38] The short dimension of the particle affords rapid charge collection (Fig. 3b). However, this design is not entirely favorable, because the dark (recombination) current of high-surface-area materials with many surface recombination sites scales with the junction area.[33,39] This can be quite large for high-aspect-ratio structures in comparison to planar devices, and increased dark current decreases both the open-circuit photovoltage and STH efficiency. This is an unresolved complication for fixed-electrode reactors that benefit from orthogonalization of light absorption and charge collection. For particle suspension reactors, this orthogonalization approach is not feasible because the particles are dispersed freely.

Reducing surface recombination and interfacial recombination is a significant challenge for development of particle suspension reactors.[40] Spherical particles are favored because they have the smallest ratio of surface area to volume compared to other particle shapes. The junction area of spherical particles is increased by only a factor of two over planar materials with the same projected area, irrespective of particle diameter. This effective roughness factor, γ, is calculated as the ratio of the surface area of the particle hemisphere ($\frac{1}{2}A_{\text{surface}}$), assuming that is the size over which one half-reaction occurs, to the area of the projected footprint of the particles ($A_{\text{projected}}$), *i.e.* $\gamma = \frac{\frac{1}{2}A_{\text{surface}}}{A_{\text{projected}}} = \frac{\frac{1}{2}\left(4\pi\left(\frac{d_{\text{part}}}{2}\right)^2\right)}{\pi\left(\frac{d_{\text{part}}}{2}\right)^2} = 2$, where d_{part} is the diameter of the particle (Fig. 5b). Smaller effective roughness factors can be attained using high-aspect-ratio particles whose long dimension is orthogonal to the direction of incident illumination,[41] $\gamma = \frac{\frac{1}{2}A_{\text{surface}}}{A_{\text{projected}}} = \frac{\frac{1}{2}(\pi d_{\text{part}})\ell_{\text{part}}}{d_{\text{part}}\cdot\ell_{\text{part}}} = \frac{\pi}{2} \approx 1.57$, where l_{part} is the length of the particle (Fig. 5c). However, this arrangement has been shown to result in increased optical reflection,[42] and maintaining this orientation in a particle suspension reactor is a considerable design challenge. In summary, unlike for the fixed-electrode design, spherical particles have advantages over anisotropic structures in terms of light absorption and charge separation when utilized in particle suspension reactors.

(D) Particle reactivity: electrocatalysis *vs.* dark recombination current

Particles located deeper in the reaction vessels will be illuminated significantly less than those located near the top of the vessels. This is likely true under any illumination conditions and any physics that describes photon propagation, absorption, and scattering. There are pros and cons to absorbing less light. It could be problematic because the open-circuit photovoltage of a particle must exceed ($E_{\text{fuel}} - E_{\text{bias}}$) in order to drive net water-splitting chemistry,[43] and the open-circuit photovoltage decreases by ($a \times (2.303RT/F) = a \times 59.2$ mV) per order-of-magnitude decrease in absorbed photon flux (at room temperature), based on the diode equation, and where a is the dimensionless diode quality factor (dqf) and has a value of one for an ideal diode. Thus, to a first approximation particles located deeper in the vessels may not be capable of splitting water, and instead will act as shunts for recombination of H_2 and O_2 to form water (Fig. 3a, inset). However, absorbing less light may not be entirely detrimental assuming even lightly illuminated particles drive net water-splitting chemistry. This is because decreased illumination results in a concurrent decrease in the open-circuit photovoltage as well as

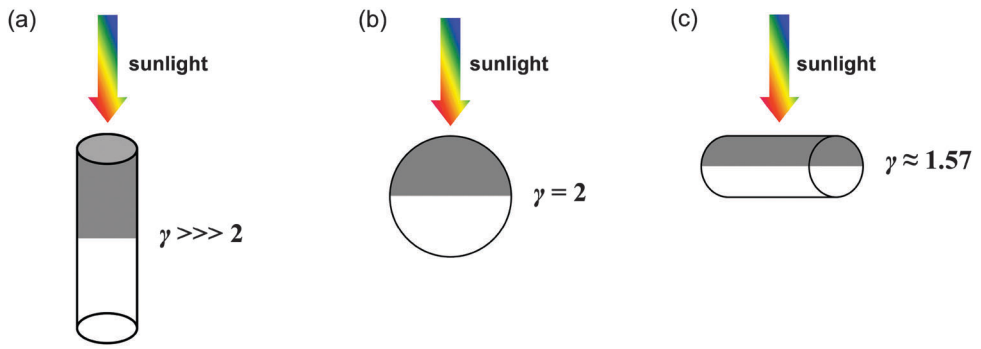

Fig. 5 Comparison of effective roughness factor (γ) among (a) high-aspect-ratio rods or wires illuminated collinear with the long dimension, (b) spherical particles, and (c) high-aspect-ratio rods or wires illuminated orthogonal to the long dimension.

a decrease in the electrocatalytic overpotential, which are effects that oppose each other. The overpotential can be approximated using the Tafel equation, which is only accurate at intermediate overpotentials, and predicts that when the current through a particle decreases by one order-of-magnitude, the overpotential decreases by the Tafel slope (units of V per order-of-magnitude change in current).[21] Because the current through a particle is directly related to the absorbed photon flux, particles deeper in the vessel are projected to exhibit both lower open-circuit photovoltages and lower overpotentials. Therefore, the efficiency of particle suspensions as a function of illumination intensity depends on the combination of the diode quality factor(s) of the light absorber(s), $\sum_{\mathrm{dqf}}$, and the combination of the Tafel slope(s) of the electrocatalyst(s), $\sum_{\mathrm{TS}}$. If $(2.303RT/F)\sum_{\mathrm{dqf}}$ is larger than $\sum_{\mathrm{TS}}$ then the STH efficiency of weakly illuminated particles (*i.e.* those deeper in the vessels) will decrease, because the photovoltage will decrease more than the required overpotential for electrocatalysis. If $\sum_{\mathrm{TS}}$ is larger than $(2.303RT/F)\sum_{\mathrm{dqf}}$ then the efficiency of weakly illuminated particles will increase, because the required overpotential for electrocatalysis will decrease more than the photovoltage. Based on state-of-the-art values for OER and HER electrocatalysts and photovoltaic light absorbers,[44,45] particles deeper in the vessels will likely operate at decreased efficiencies.[43] Again, this assumes that Tafel analysis is valid at small overpotentials and that the photovoltage is large enough to drive net water-splitting chemistry. Moreover, this assumes that the rate-limiting recombination steps are independent of light intensity, which may not be the case under strong illumination conditions where high-level injection and equal-concentration second-order recombination become dominant.[46]

(E) Colloidal particle dispersion

Particle suspensions for solar PEC water splitting can consist of fully dispersed colloids or particulate suspensions, assuming convection is sufficient to prevent sedimentation. For particles that are fully dispersed as colloids, their stability toward flocculation and sedimentation is affected by several primary factors. Particles are driven together by Brownian motion (quiescent) or shear forces (dynamic) while local forces can be attractive (dispersion) or repulsive (electrostatic).[47] Any characteristic that affects particle–particle interactions will affect colloidal stability, irrespective of particle size. Moreover, colloids can form from any phase of matter. The most relevant for solar PEC water-splitting reactors are the solid light-absorber particles and gas bubbles.[48] The following discussion on dispersion applies to both types, with the main distinction being the result of destabilization: solid particles coalesce into a solid that settles to the bottom of a vessel through gravity, while bubbles flocculate into larger bubbles that escape into the gas phase. In the absence of electrostatic repulsion, Brownian motion results in interparticle condensation and eventual loss of colloidal stability on a timescale determined by the diffusion rate. The primary factors affecting the diffusion rate are the particle dimensions and solution viscosity, related through the Stokes–Einstein equation.

The basic forces between charged colloidal particles in a liquid are described by Derjaguin–Landau–Verwey–Overbeek (DLVO) theory.[49,50] According to this theory the stable distance between two particles surrounded by an electrical double layer is determined by the balance between van der Waals attraction and electrostatic repulsion. In the case of solar PEC water-splitting reactors there are several dominant factors that influence this balance. The ionic strength of the aqueous electrolyte plays a direct role, where the higher the ionic strength the greater the tendency to flocculate due to electrostatic shielding of repulsive forces that would normally maintain a separation between charged particle surfaces. Stability also depends on surface composition and charge which are affected by illumination, temperature, electrolyte composition, impurities, defects, and adsorbed molecules (*e.g.* reactants, products, ligands). A colloid will be more stable due to repulsion when the particles are highly charged and present more sterically hindered surfaces. However, the characteristics of each particle are not static and are affected by optical intensity, spectral distribution, and temperature which each vary during the day and with seasons, and may also be affected by chemical reactions. The stability of colloidal solutions over wide concentration ranges are also influenced by components in the solution that adsorb to the particle surfaces as well as by interparticle repulsions, resulting in varying stabilities with particle and molecular loadings. This is particularly relevant to Type 2 reactors that require a solution redox shuttle to mediate charge, which in several cases described below has been shown to adsorb to particle and cocatalyst surfaces.

When the concentration of particles is large, stability can be observed due to high charge density and/or molecular surface area density that is very repulsive, stabilizing the colloidal solution due to electrostatic and entropic effects. For a dilute solution with a low concentration of particles, the colloidal solution can also be stable due to kinetic limitations on nucleating a floc. For intermediate concentrations, aggregation is more likely to be favored due to the more complex balance of relevant factors that affect stability and often lead to eventual coagulation. A particle concentration that is optimized for optical absorption and scattering may be completely incompatible with the particle concentration and electrolyte composition required to maintain colloidal stability, leading to limitations on achievable performance. However, colloidal solutions are not quiescent under operating conditions even if there is no imposed flow, so bubbles and solid particles can affect each other. Bubble coalescence and migration into the gas phase imparts flow and shearing activity to the electrolyte and this kinetic energy can increase the tendency of solid particles to flocculate by driving them closer together. In summary, there is a complex interplay of various phenomena that determine whether a colloidal solution of particles is stable and appropriate for a solar PEC water-splitting device.

(F) Cocatalyst materials and selective catalysis

Electrocatalysts are necessary components of PEC water-splitting devices, because it is unlikely that a given light-absorber material

also facilitates rapid redox chemistry. Electrocatalysts chosen specifically to catalyze the desired redox chemistry and used in conjunction with a light-absorber material are termed cocatalysts. Light-absorber materials generate power through sunlight absorption while cocatalysts decrease the activation energy for the desired fuel-forming reactions, which is manifest by an increased exchange current density and decreased electrocatalytic overpotential. Because cocatalysts are in physical contact with light-absorber materials, sunlight-transmitting cocatalysts are desired.

Many electrocatalyst materials and molecules have been examined as cocatalysts for application in solar PEC water splitting. An extensive list is beyond the scope of this review paper, and various reviews already exist.[12,44,45,51–59] Instead, this section focuses on unique cocatalysts and materials architectures that are specific and/or beneficial to the particle suspension reactors described herein. In addition, this section explains the role of the cocatalysts in a particle suspension reactor where at least four redox-active chemical species exist near any region of a particle, at any time. Thus, the cocatalyst must be selective for one half-reaction in the presence of reaction products from another half-reaction(s). This requirement is unique to particle suspension reactors, because in fixed-electrode designs the reaction products are physically separated and by design crossover of reaction products is small.

Traditionally the surfaces of light-absorber semiconductor particles do not contain active sites for efficient electrocatalytic generation of H_2 or O_2. Cocatalysts are desired, but fabricating anisotropic distributions of cocatalysts for the HER, the OER, and/or redox shuttle electrochemistry on nanometer-to-micron-sized particles is challenging. One option is to use PEC deposition where cocatalysts are photoelectrochemically deposited at the sites of preferential collection of photogenerated electrons or holes. Deposition of catalysts on surfaces (cathodic deposition for HER catalysts and anodic deposition for OER catalysts) aligns the intrinsic carrier-selective sites to the electrocatalytic sites, which may be advantageous to charge collection and electrocatalysis, and distinguishes the locations for the electron-selective and hole-selective surface sites to attenuate intraparticle shunts. Ag^{+}, $AuCl_4^{-}$, and $PtCl_6^{2-}$ are often used as precursors for cocatalyst deposition on electron-transfer sites, while Pb^{2+}, Mn^{2+}, and Ni^{2+} are used for hole-transfer sites.[60–62] For example, selective PEC deposition on $BiVO_4$ was attained on the {010} facets using solution-phase cathode catalyst precursors and on the {110} facets using anode catalyst precursors (Fig. 6a).[61] Moreover, through use of surfactants that preferentially adsorbed onto certain crystal facets of Cu_2O and ZnO, deposition of Au particles was shown to be inhibited on these facets and thus was selective to the other facets (Fig. 6b).[63] Pt nanoparticles have been selectively deposited on the tips of CdS nanorods,

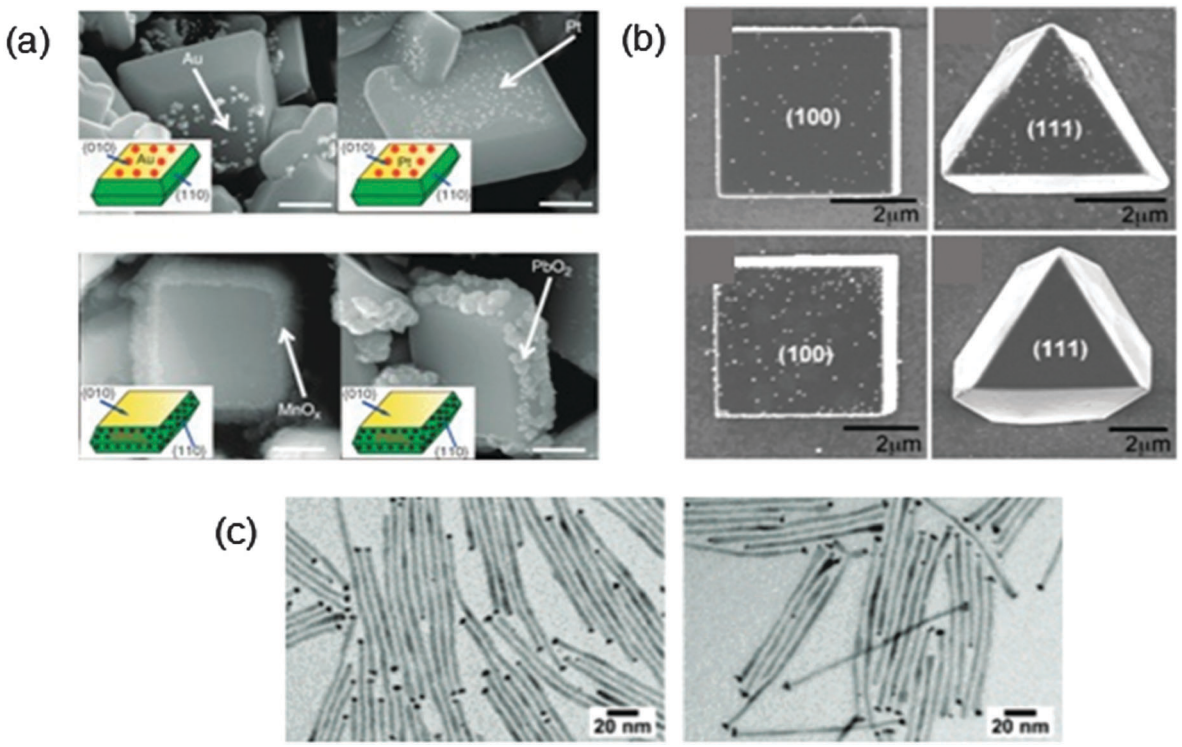

Fig. 6 (a) Scanning-electron micrographs of micron-sized $BiVO_4$ crystallites after facet-selective PEC deposition of the indicated materials (scale bars are 500 nm). Reprinted by permission from Macmillan Publishers Ltd: Nature Communications (59), copyright 2013. (b) Scanning-electron micrographs of micron-sized Cu_2O crystallites with Au deposited in the absence (top) or in the presence (bottom) of sodium dodecylsulfate. Adapted with permission from C. G. Read, E. M. P. Steinmiller, K. S. Choi, *J. Am. Chem. Soc.*, 2009, **131**, 12040–12041.[63] Copyright 2009 American Chemical Society. (c) Transmission-electron micrographs of PtNi (left) and PtCo (right) chemically deposited on the tips of CdSe nanorods. Reprinted with permission from S. E. Habas, P. Yang, T. Mokari, *J. Am. Chem. Soc.*, 2008, **130**, 3294–3295.[64] Copyright 2008 American Chemical Society.

which presents a different crystal facet than along their sidewalls (Fig. 6c).[64] As a demonstration, this method was used to promote H_2 evolution from the as-deposited Pt tips of CdSe/CdS core–shell nanorods.[65]

While *selective deposition* of cocatalysts may be useful for driving reactions at preferred locations on the light-absorber materials surfaces, *selective catalysis* is also extremely important in order to prevent recombination shunts due to unwanted reactions with reaction products.[40] Size exclusion has been remarkably successful in realizing selective catalysis for demonstrations of solar PEC water splitting using particle suspensions. Domen and colleagues reported that thin shells of amorphous, porous oxides, *e.g.* Cr_2O_3, selectively facilitate proton transport to the HER cocatalysts while allowing H_2 to exit the structure and size-excluding larger species like O_2 (Fig. 7a and b).[12,51,66] In addition, Frei and colleagues showed that solid silica shells (2 nm thick) with embedded electrically conductive organic molecules afforded protonic conduction through the silica matrix and electronic conduction through the organic groups (Fig. 7c and d).[13] Larger species like O_2 were size excluded from entering into and through the silica. A materials fabrication-independent scenario has also been proposed by Abe, Kudo, Matsumura, and colleagues, where molecular redox shuttles in solution, *e.g.* IO_3^- and Fe^{3+}, bind to the surface of the light-absorber material thereby attenuating reduction of these chemical species by H_2 or photogenerated electrons in the material.[67–70]

It may also be possible to achieve selective catalysis *via* engineering the electron-transfer kinetics at the surface of the particles. Selective redox-shuttle catalysis will occur due to the small aqueous solubility (Henry's law) constants for the water-splitting reaction products, *i.e.* H_2 and O_2, and large activation overpotentials for the HER and the OER at redox-shuttle cocatalysts, which will likely be carbon materials or the light-absorber surfaces themselves. To prevent mass-transport-limited reactivity of the redox shuttle at these cocatalysts the tradeoff between cocatalyst area and the rate of forced convection needs to be determined. Selective catalysis at the fuel-forming electrocatalysts will occur due to mass-transport limitations of the redox shuttle, because the area of the efficient HER and OER cocatalysts will be small and the diffusion coefficient of many redox shuttles is at least an order-of-magnitude smaller than that of protons, hydroxide ions, and water. These engineering approaches to selective catalysis will be successful only through careful choice of cocatalyst material, electrochemically active cocatalyst area, redox-shuttle concentration, and rate of forced convection, but will benefit in that advanced nanoscale materials design and synthesis required to size exclude reaction products is not required.

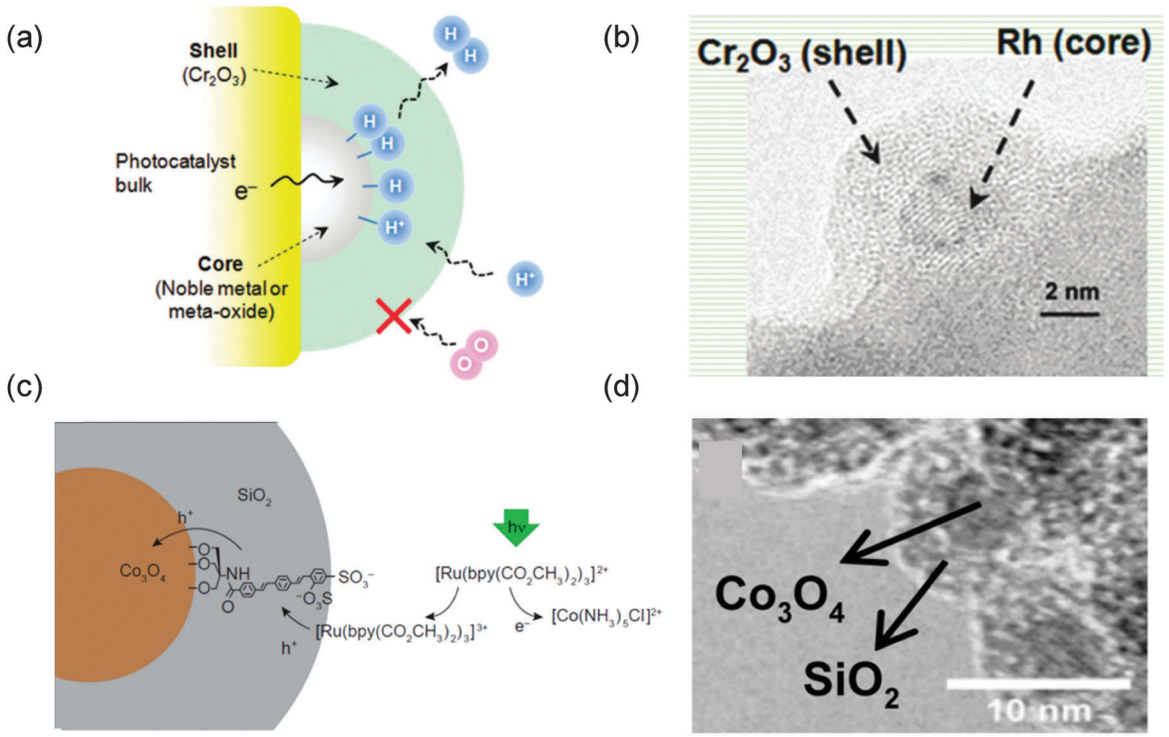

Fig. 7 (a) Schematic of materials catalyst architecture used to size exclude molecules from electrocatalysts and (b) accompanying transmission-electron micrograph. Reprinted with permission from K. Maeda, K. Domen, *J. Phys. Chem. Lett.*, 2010, **1**, 2655–2661.[12] Copyright 2010 American Chemical Society. (c) Schematic of material–molecule hybrid catalyst architecture used to size exclude molecules from electrocatalysts and (d) accompanying transmission-electron micrograph of the materials. Reprinted/adapted with permission from A. Agiral, H. Sen Soo, H. Frei, *Chem. Mater.*, 2013, **25**, 2264–2273.[13] Copyright 2013 American Chemical Society.

IV. Efficiency metrics

(A) System STH efficiency

The most important performance metric for a practical solar PEC water-splitting technology is the STH efficiency, which is a ratio of the net power output to the solar power input. Two versions of this equation that contain variables that could be measured experimentally and are most relevant to particle suspension reactors follow:

$$\eta_{\mathrm{STH}} = \frac{2F \cdot v_{\mathrm{coll}}(E_{\mathrm{fuel}} - E_{\mathrm{bias}})}{P_{\mathrm{in}} \cdot A_{\mathrm{reactor}}} \quad (1)$$

$$\eta_{\mathrm{STH}} = \frac{N_{\mathrm{A}} \cdot c_{\mathrm{p}} \cdot \ell \cdot \phi_{\mathrm{coll}} \cdot I_{\mathrm{particle}}(E_{\mathrm{fuel}} - E_{\mathrm{bias}})}{P_{\mathrm{in}}} \quad (2)$$

where in the first equation, the factor of two is the stoichiometry of electrons required to generate H_2 from H^+, F is Faraday's constant (96 485 C mol^{-1}), v_{coll} is the rate of collection of H_2 (mmol product s^{-1}), E_{fuel} is the potential available from the reaction products when utilized in an electrochemical cell (V; *e.g.* 1.229 V for aqueous water splitting at 25 °C and under standard-state conditions), E_{bias} is the bias applied to the system (V), P_{in} is the input solar irradiance (mW cm^{-2}; *e.g.* 100 mW cm^{-2}, or 1 Sun intensity, of air mass (AM) 1.5G sunlight), and $A_{reactor}$ is the projected geometric area of the reactor perpendicular to the direction of illumination (cm^2).[71] Because this metric is a measure of the power output based on the *solar* power input, the E_{bias} term is subtracted from E_{fuel} and not added to P_{in}. Another review paper published in this journal issue by Coridan *et al.* describes this and other efficiency definitions.[72] These efficiency equations are only applicable when $E_{bias} < E_{fuel}$, because otherwise no sunlight energy is stored in the chemical bonds of H_2 and O_2. By analogy to fixed-electrode STH efficiency measurements, if the average net current through an illuminated particle is known, the second equation may be useful, where N_A is Avogadro's constant (6.022×10^{23} mol^{-1}), c_p is the concentration of particles in solution (mol cm^{-3}), ℓ is the reactor height in the direction of illumination (cm), $\phi_{collection}$ is the quantum yield (QY) for external collection of a stream of H_2, and $I_{particle}$ is the average net current through a single particle (A).

Traditionally, gases from the headspace(s) of reactor vessels are collected using flow systems. The quantity of collected gas is often used to approximate the amount of products produced, and more thorough analyses identify the product distributions using a gas chromatograph and/or mass spectrometer. Many fixed-electrode measurements do not identify the products of their reactions and instead rely on current through the electrodes, assuming the yield for electron-transfer reactions forming H_2 or O_2 is unity and the yield for collection of pure products is unity; an analogous measurement for particle suspensions has also been used for a Type 2 reactor design. The two vessels were connected ionically with a Nafion membrane and electrically using electrodes inserted into each vessel.[67] Using a two-electrode potentiostatic measurement poised at the initial, dark open-circuit potential, an approximate H_2/O_2 generation rate under illumination was obtained by measuring the current through the circuit due to equilibration of the redox shuttles.

The maximum theoretical efficiency for both reactor designs is the single-junction solar-cell detailed-balance limit of ~31%, which can be attained with a 1.1–1.4 eV bandgap material.[73] This theoretical single-junction efficiency limit holds for the Type 2 (tandem-junction) reactor, in the absence of spectral splitting, because the vessels are arranged side-by-side, as in Fig. 1b, and not stacked optically in series which would result in a substantially larger theoretical efficiency limit. In reality these efficiency limits will be much smaller due to required activation overpotentials, which are present in any device for PEC water splitting irrespective of the reactor type.[4–7,74,75] Solar water-splitting reactors do not necessarily require that the evolved O_2 is collected. However, ideally H_2 and O_2 should be evolved in the 2 : 1 mol/mol or v/v stoichiometry expected for water splitting. If the amount of O_2 generated is quantified, any discrepancy from the ideal 2 : 1 stoichiometry implies leaks in the reactor or imperfect water-splitting chemistry and undesired additional side reactions, which may not be sustainable over the long-term if the "missing" charges performed irreversible redox chemistry with the particles.

(B) Bias assistance

In addition to the requisite input of sunlight (*e.g.* simulated 1 Sun AM 1.5G illumination), several other energy inputs can be introduced to bias the system. These biases can be separated into five categories: chemical, electrical, optical, pressure, or thermal (Fig. 8). Electric potential bias is not described in detail below because it is only pertinent to fixed-electrode designs. The purpose of any of these biases is to slow charge recombination, increase the yield of charge separation or charge collection, and/or increase rates of electrocatalysis.

Chemical bias. When particle suspensions are evaluated, a chemical bias is particularly useful because it obviates rapid and undesired recombination reactions (Fig. 8b). These chemical biases are attained through corrosion or passivation of the particle itself or *via* redox chemistry with redox-active sacrificial molecules or materials in the electrolyte or at the material surface, *e.g.* alcohols, sulfite, Ag^+, amines, $[Co(NH_3)_6]^{3+/2+}$, ethylenediaminetetraacetate ($EDTA^{2-}$). Sacrificial reagents quench photo-excited particles *via* electron-transfer reactions so that the particle subsequently resembles a ground-state particle with one additional or one fewer electron. This state is essentially identical to that formed through electrical bias (*e.g.* from an electrode), and so a chemical bias is analogous to an electrical bias, which must be taken into consideration when calculating the STH efficiency. The biasing species are often termed sacrificial because their electrochemical reactivity is irreversible or they have extremely slow reverse reaction rates. They react with the illuminated particle and remove one of the electronic charge carriers, *i.e.* an electron or a hole. The remaining electronic charge carrier can then perform the desired fuel-forming redox half-reaction, *i.e.* the HER or the OER. These chemical biases constitute a non-regenerative, non-solar-energy input, because additional energy is required to synthesize and introduce the

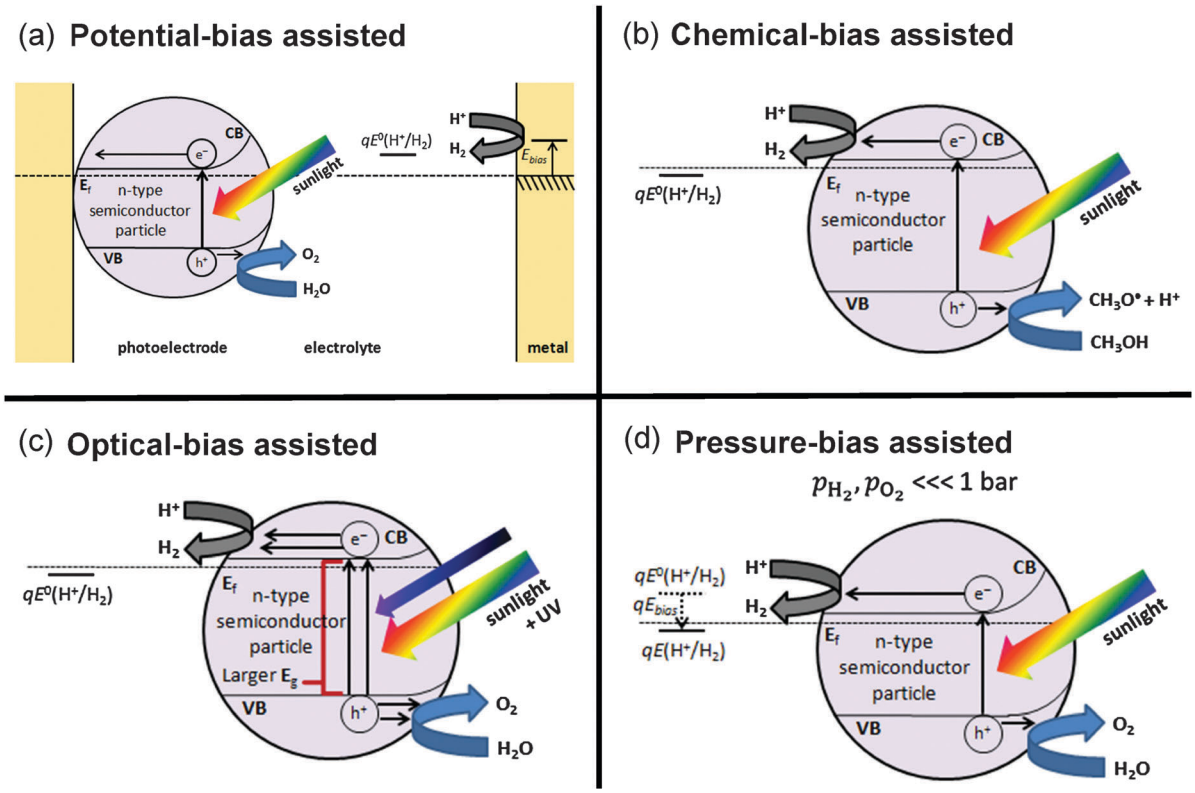

Fig. 8 Schematic representations of bias-assisted mechanisms for solar PEC water splitting using an n-type semiconductor. (a) Potential bias: Electrical bias for fixed electrodes modulates the Fermi level (E_f) of the illuminated photoanode so that it is sufficient to drive net H_2 evolution; this bias (E_{bias}) compensates for the difference in electrochemical potential between E_f and $qE^0(H^+/H_2)$. (b) Chemical bias: Sacrificial reagents like methanol are introduced into the electrolyte and reductively quench photo-excited particles, promoting H_2 evolution. (c) Optical bias: Ultraviolet light adds additional energy to the system allowing larger band-gap ultraviolet-light-absorbing particles to be used. (d) Pressure bias: A positive E_{bias} is introduced by decreasing the partial pressure of H_2 and/or O_2 gas in the headspace which removes dissolved H_2 and O_2 and makes $E(H^+/H_2)$ and/or $E(O_2/H_2O)$ more thermodynamically favorable.

sacrificial reagents. As a consequence, a potential that is less than E_{fuel}, and often less than zero, is stored in the chemical bonds of the reaction products, *i.e.* H_2 and O_2.

Sacrificial reagents are, however, useful for investigating charge-transfer processes across particle/electrolyte interfaces and subsequent electrocatalysis in bulk electrolytes. Sacrificial reagents perform rapid electron transfer for one half-reaction so that the behavior of the other fuel-forming half-reaction can be isolated and investigated without complications from recombination of electrons and holes.[76–80] However, these photogalvanic-type methods typically do not store net photon energy in chemical bonds. Thus, sacrificial reagents should only be used to learn more about the fundamental charge-transfer reaction mechanisms and electrocatalysis, and any chemistry that results from their use should not be considered useful solar-energy conversion chemistry.

Optical bias. An optical bias is present when a non-solar optical input is supplied, typically ultraviolet light, in addition to solar illumination in order to assist the water-splitting reactions or drive them entirely (Fig. 8c). Unlike a chemical or electrical bias, the energy in an optical bias is lost irrespective of whether it is used by the particle, *e.g.* regardless of whether the photon is absorbed. Thus, when calculating the STH efficiency the total optical bias must be amortized over every charge that results in net H_2 and O_2 evolution. This non-solar optical input is typically supplied by high-energy photons and differs from the incident (simulated) solar illumination, which is the only relevant source of power input for a *solar* PEC water-splitting reactor.

Pressure bias. A pressure bias is another type of chemical bias. It relies on partial evacuation of H_2 and/or O_2 from the headspace and out of solution, or dilution of the headspace with another (carrier) gas, which makes the thermodynamics for net water-splitting redox chemistry more favorable (Fig. 8d). Although E_{fuel} for aqueous water splitting at 25 °C and under standard-state conditions is 1.229 V, the photo-potential required to split water by solar illumination depends on the partial pressure of H_2 and O_2. This is important because in many reports of solar PEC water splitting, H_2 and O_2 were evolved under reduced pressure, which constitutes a non-zero E_{bias}. According to the Nernst equation, the bias potential can be estimated as 29.6 mV per order-of-magnitude reduction in H_2 pressure from 1 bar, and 14.8 mV per order-of-magnitude reduction in O_2 pressure from 1 bar. As an example, a report by Domen and colleagues using $Rh_{2-y}Cr_yO_3$-modified GaN:ZnO particles was specifically not operated under a reduced pressure, but instead in a static air atmosphere.[81] Under this condition the

initial potential required to impart water splitting was also not 1.229 V but rather approached $-\infty$ V because no H_2 was present and therefore $E_{bias} \rightarrow \infty$ V. It is often assumed that during rapid water splitting under an ambient atmosphere, enough H_2 and O_2 exist near the surface of the electrodes (or particles) so that generally the standard potential, E^0_{fuel}, is an accurate approximation of E_{fuel}.[82] It is unclear if this approximation holds when H_2 and/or O_2 are present at reduced partial pressures. To assess whether particle suspensions are suitable for use in an actual solar PEC water-splitting reactor, they should be evaluated in the presence of H_2 at 1 bar pressure above the HER reactor and O_2 at 1 bar pressure above the OER reactor. Formation of products can then be measured by a change in gas volume or a change in pressure, along with quantification of the purity of the product gas streams.

Thermal bias. No standard temperature has been set for solar PEC water-splitting applications. However, because most solar installations will operate at temperatures greater than room temperature, it is best to define the standard potential, E^0_{fuel}, using this elevated temperature. Then, use of other temperatures will constitute a bias. This is particularly important, because apparent activation energies for solar PEC water splitting using certain particles were reported to be 8–15 kJ mol^{-1}, implying that thermal bias can potentially increase the rate of electrocatalysis and the STH efficiency for solar PEC water splitting.[46] For the purpose of this review, 25 °C was used as the standard temperature, because that is approximately the temperature utilized for the laboratory-scale demonstrations reported below.

(C) Spectral response (quantum yield)

Although ultimate STH efficiency is the parameter that dictates effectiveness of solar PEC water-splitting, research demonstrations using particle suspensions do not often report the STH efficiency and instead report the (monochromatic) spectral response. The spectral response is typically performed as a function of optical excitation wavelength with values ranging from 0 to 1 at each wavelength. This value quantifies the fraction of product collected based on the number of photons incident or absorbed.[83] This information can be used along with the spectrum of the simulated solar illumination source to calculate the STH efficiency by weighting the simulated solar spectrum by the incident (external) spectral response and integrating. If the yields are reported at only several excitation wavelengths, integration over only those selected wavelengths results in a lower bound to the STH efficiency. Most demonstrations of solar PEC water splitting using particle suspensions (reported below) only indicate the spectral response at one wavelength or one small range of wavelengths. In either case, the calculated value for the lower bound of the STH efficiency is far from the true STH efficiency and thus is not a meaningful approximation of the actual STH efficiency. Instead, for most solar PEC water-splitting demonstrations, the monochromatic, or near-monochromatic, spectral response is reported, often as an external (incident) quantum yield (EQY) based on the incident photon flux (Table 1). This is not often converted into an internal (absorbed) quantum yield (IQY) but could if absorption by the particle suspensions was determined using a spectrophotometer equipped with an integrating sphere. Instead, most demonstrations utilize highly concentrated suspensions that are assumed to absorb nearly all incident above-bandgap light and in which case IQY $\approx$ EQY.

(D) Alternative characterization strategies

Unlike for fixed electrodes, few means to characterize the performance of particle suspensions for solar PEC water splitting exist.[71,83] For example, although STH efficiency can be determined through quantification of the amount of reaction products, the current–potential behavior of individual particles or particle suspensions has not been reported.

The overall quantum yield for product detection (*i.e.* spectral response for a given range of illumination wavelengths) can be written as the product of the quantum yields of several individual steps: optical absorption, charge separation, charge transport, fuel-forming catalysis, and product collection. To glean more information into the causes of the observed STH conversion efficiencies and overall quantum yields for these particle suspensions, quantitative values for the quantum yields for each sub-step are beneficial. This, however, is not straightforward because each of these steps occurs in/on individual isolated particles. Measuring the performance of each process requires new characterization methods specific to particle suspensions.

For example, surface photovoltage (SPV) measurements have been used to investigate the interplay of charge separation and charge recombination to cocatalyst materials. An advantage of this technique is that it can be used to measure processes in/on individual particles without the necessary requirement of a redox agent. The changes in surface photovoltage as a function of incident photon energy reveal locations with altered yields for charge separation, charge collection, and/or charge recombination.[84–87] Another review paper published in this journal issue by Esposito *et al.* describes additional characterization techniques relevant to these types of designs.[88] Alternatively, particles are often cast onto conductive electrodes like fluorine-doped tin oxide (FTO) or gold films to evaluate their ensemble photoelectrochemical and transient spectroscopic behavior in a fixed-electrode form factor.[89] However, it is unclear to what extent the behavior observed using fixed electrodes corresponds to the behavior of particle suspensions.

V. Experimental demonstrations

Concerted research efforts in PEC date back to the seminal work by Brattain, Garrett, Gerischer, Boddy *et al.* in the 1950s–1960s using materials from the photovoltaics community and metal-oxide materials in fixed-electrode arrangements.[53,90–92] Several decades later, research into PEC water splitting using particle suspensions was reported.[93–95] Although initial reports were promising,[96–100] it quickly became apparent that the fixed-electrode demonstrations were far more efficient.[52,63,64,90] Thus, although particle suspension designs remain an active area of

research, many more research advances have been realized using fixed-electrode demonstrations. Notwithstanding, there have been many demonstrations of PEC water splitting using particle suspensions illuminated with only ultraviolet light. Recently this topic has been extensively reviewed,[12,46,52–54,101–105] and it is beyond the scope of this review paper.

Suspensions for solar PEC water splitting typically contain particles with diameters on the nanometer to micron size ranges. The first demonstrations of PEC water splitting using particle suspensions were reported in the late 1970s and early 1980s and utilized TiO_2, where upon ultraviolet-light illumination redox chemistries occurred that are amenable to a Type 1 reactor.[93–95] Most metal-oxides have bandgap energies that are too large to absorb visible light, yet many of them are the most stable PEC materials.[106] To extend the absorption of metal-oxides into the visible spectral region, many metal-oxides have been doped with other transition metals or had some or all of the oxygen atoms replaced with pnictogens, other chalcogenides, or halides.[54,107]

The first demonstration of PEC water splitting at the expected 2 : 1 v/v stoichiometric ratio of H_2 and O_2 and that required redox shuttle chemistries amenable to a Type 2 reactor were reported in 2001, over twenty years later, by Arakawa and colleagues.[23] This demonstration also required ultraviolet light excitation (λ > 300 nm) and consisted of a suspension of Pt-loaded anatase TiO_2 (bandgap energy (E_{bg}) = 3.2 eV) HER particles, rutile TiO_2 (E_{bg} = 3.0 eV) OER particles, and an IO_3^-/I^- redox shuttle in pH 11 NaI aqueous electrolyte.

The first non-oxide particle for PEC water splitting *via* a process amenable to a Type 1 reactor was reported in 2005 by Domen and colleagues.[108] The authors described β-Ge_3N_4 particles (E_{bg} = 3.8–3.9 eV) loaded with RuO_2 HER cocatalysts (1 wt%) in pH 0 H_2SO_4 aqueous electrolyte which were reported to evolve H_2 and O_2 in a 2 : 1 v/v stoichiometry when illuminated by ultraviolet light, with an external quantum yield of ~9% at an excitation wavelength of 300 nm (EQY_{300nm}). Little N_2 was produced (<0.3 mol% of the H_2 produced), which is a common degradation product of nitride materials, and >6 turnovers were reported per particle.

Some additional unique examples of PEC water splitting using particle suspensions, a redox shuttle(s), and ultraviolet light excitation include the following. A partially solid-state redox shuttle, MnO_4^{2-}(aq)/MnO_2(s), was used with TiO_2 particles in pH 13 NaOH aqueous electrolyte to impart PEC water splitting under ultraviolet light excitation.[109] Another demonstration required photoexcitation of the redox shuttle in order to evolve H_2. A suspension of RuO_2-loaded (3 wt%) WO_3 (E_{bg} ≈ 2.7 eV) OER particles in an aqueous electrolyte consisting of 1.4 mM $Fe^{III}_2(SO_4)_3$, 5.7 mM $Fe^{II}(SO_4)$, and 29 mM H_2SO_4 was reported to evolve stoichiometric H_2 and O_2 under concomitant photoexcitation of WO_3 (>400 nm) and Fe^{2+} (<280 nm).[110] Lastly, a Type 2 reactor design was reported that connected the two vessels ionically using a Nafion membrane and electrically using a wire that contacted two Pt electrodes, one immersed in each vessel. Pt-loaded (0.9 wt%) rutile TiO_2 HER particles and 2 M KBr in pH 2.4 aqueous electrolyte were confined to one electrochemical cell and rutile TiO_2 OER particles and 6.5 mM $FeCl_2$ (with some Fe^{3+} generated photoelectrochemically) in pH 2.4 aqueous electrolyte were confined to the second electrochemical cell.[67] This design afforded use of two different redox shuttles, *i.e.* $Br_3^-/Br_2/Br^-$ and Fe^{3+}/Fe^{2+}.

Demonstrations of visible-light-driven PEC water splitting are plotted in Fig. 9 as a function of the year of the report. Each of these demonstrations is described in greater detail below in the text. For each of the unique light-absorber particle(s) (and redox shuttle) combinations, data relevant to the demonstration with the highest reported quantum yield are tabulated in chronological order in Tables 2–5 based on each type of system: single particles, solid-state tandem particles, two particles with an iodine-based redox shuttle, and two particles with a non-iodine-based redox shuttle.

(A) Single particles

This section compiles and describes demonstrations of solar PEC water splitting using particle suspensions where *each*

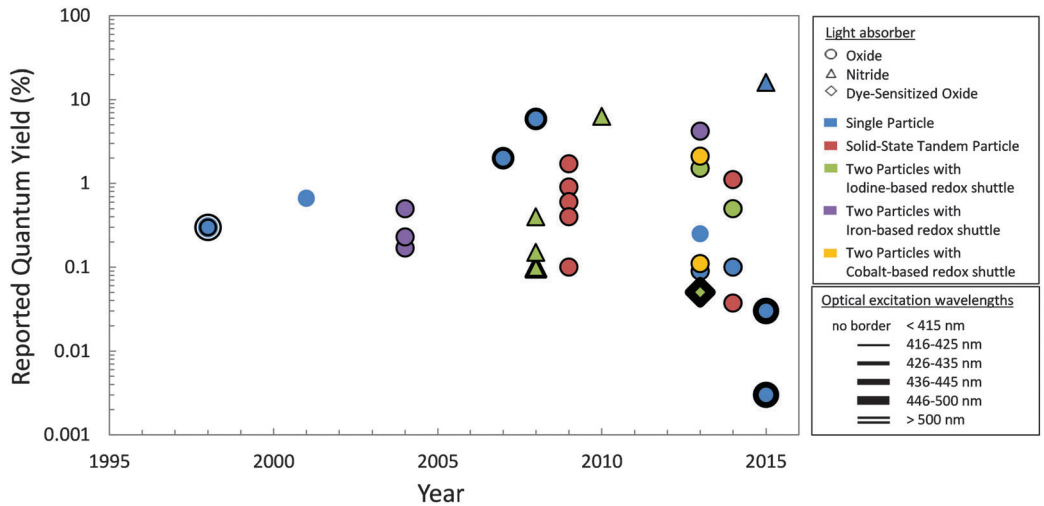

Fig. 9 Maximum reported quantum yields on a semi-logarithmic scale for literature demonstrations of visible-light-driven PEC water splitting categorized by type of light-absorber material (shape) and system (color), and wavelength of light used to excite the particles (border thickness).

Table 2 Reports of visible-light-driven water splitting using suspensions consisting of one type of particle[a]

Light-absorber	HER cocatalyst (wt%)	OER cocatalyst (wt%)	Aqueous electrolyte (pH)	Activity measurement: Illumination[b] (irradiance (mW cm^{-2}), wavelength (nm))	H_2, μmol h^{-1}	O_2, μmol h^{-1}	Quantum yield, % (wavelength (nm)) and/or STH efficiency, %	Year[ref]
Cu_2O	None	*None*	Pure water	Xe (n.r., ⩾460)[c]	2	1	0.3 (550–600)	1998[111]
$In_{1-x}Ni_xTaO_4$	NiO_y (1.0)	None	Pure water	Xe (n.r., >420)	17	8.3	0.66 (402)	2001[115]
$(Zn_{1+x}Ge)(N_2O_x)$	$Rh_{2-y}Cr_yO_3$	None	Pure water	Hg (n.r., >400)	320	160	2.0 (420–440)[d]	2008[126]
$(Ga_{1-x}Zn_x)(N_{1-x}O_x)$	$Rh_{2-y}Cr_yO_3$	None	H_2SO_4 (3)	Hg (n.r., >400)	930	460	5.9 (420–440)[d]	2008[122]
$Au/TiO_2/Al_2O_3$	Pt	Co-OEC[e]	K_3BO_3 (9.6)	Xe (300, AM 1.5G)	~0.4	~0.2	~0.25 (>410)	2013[127]
ZrO_2–TaON	RuO_x/Cr_2O_3	IrO_2	Pure water	Hg (n.r., >400)	~3	~1.5	~0.1 (420)	2013[128]
Si/TiO_2	Pt	IrO_x	H_2SO_4 (0.52)	Xe (150, AM 1.5G)	2.1	1.1	0.12 STH	2013[129]
$SrTiO_3$:Rh,Sb	IrO_2 (3.0)	IrO_2 (3.0)	H_2SO_4 (3)	Xe (100, >440)	3.4	1.5	0.1 (420), 0.1 STH	2014[130]
CoO	**None**	**None**	**Pure water**	**Xe (100, AM 1.5G)**	**n.r.**	**n.r.**	**5 STH**	**2014**[131]
C_3N_4/CDots[f]	**None**	**None**	**Pure water**	**Xe (70–100, >420)**	**46**	**23**	**16 (420), ~2 STH**	**2015**[132]
$LaMg_xTa_{1-x}O_{1+3x}N_{2-3x}$	*$RhCrO_y$*	*None*	*Pure water*	*Xe (n.r., ⩾420)*	*~1*	*~0.5*	*0.03 (440 ± 30)*	*2015*[133]
$CaTaO_2N$	$RhCrO_y$	None	Pure water	Xe (n.r., ⩾420)	~0.12	~0.06	~0.003 (440 ± 30)	2015[134]

[a] For each light-absorber material only the highest reported quantum yield is included. Bold typeface indicates the designs with the largest reported quantum yield and largest reported STH efficiency. Italicized typeface indicates the design that absorbs at the longest wavelength. [b] Xe = 300 W xenon lamp with a Pyrex cell; Hg = 450 W high-pressure mercury lamp with a Pyrex cell. [c] n.r. = not reported. [d] Used Xe lamp. [e] Co-OEC = Cobalt-based oxygen-evolution catalyst. [f] CDots = carbon nanodots.

Table 3 Reports of visible-light-driven water splitting using suspensions consisting of pairs of particles in solid-state contact[a]

Light absorbers	HER cocatalyst (wt%)	OER cocatalyst	Aqueous electrolyte (pH)	Activity measurement: Illumination[b] (irradiance (mW cm^{-2}), wavelength (nm))	H_2, μmol h^{-1}	O_2, μmol h^{-1}	Quantum yield, % (wavelength (nm)) and/or STH efficiency, %	Year[ref]
$SrTiO_3$:Rh/$BiVO_4$	**Ru (1)**	**None**	**H_2SO_4 (3.5)**	**Xe (100, >420)**	**40**	**19**	**1.7 (420)**	**2009**[135]
$SrTiO_3$:Rh/Bi_2MoO_6	Ru (1)	None	H_2SO_4 (3.5)	Xe (100, >420)	12	5.2	~0.9 (420)	2009[135]
$SrTiO_3$:Rh/TiO_2:Cr,Sb	Ru (1)	None	H_2SO_4 (3.5)	Xe (100, >420)	6.7	3.3	~0.6 (420)	2009[135]
$SrTiO_3$:Rh/WO_3	Ru (1)	None	H_2SO_4 (3.5)	Xe (100, >420)	5.7	2.4	~0.4 (420)	2009[135]
$SrTiO_3$:Rh/$AgNbO_3$	Ru (1)	None	H_2SO_4 (3.5)	Xe (100, >420)	1.9	0.7	~0.1 (420)	2009[135]
$SrTiO_3$:La,Rh/Ta_3N_5	*Ru (0.2)*	*IrO_x*	*H_2SO_4 (3.9)*	*Xe (100, 420–800)*	*~48*	*~24*	*1.1 (420), 0.037 STH*	*2014*[139]
$ZnRh_2O_4$/Ag/$Ag_{1-x}SbO_{3-y}$[c]	None	None	Pure water	Xe (n.r., >460)	~0.004	~0.002	0.037 (420)	2014[140]
p-GO:N/n-GO:N[d]	None	None	Pure water	Xe (n.r., 420–800)[e]	~0.6	~0.3	n.r.	2014[141]

[a] For each combination of light-absorber materials only the highest reported quantum yield is included. Bold typeface indicates the design with the largest reported quantum yield. Italicized typeface indicates the design that absorbs at the longest wavelength. [b] Xe = 300 W xenon lamp with a Pyrex cell. [c] Ag acts as a solid-state mediator for electron transfer. [d] GO = graphene oxide. [e] n.r. = not reported.

Table 4 Reports of visible-light-driven water splitting using suspensions with two particles and an iodine-based redox shuttle[a]

HER light absorber	HER cocatalyst (wt%)	OER light absorber	OER cocatalyst (wt%)	Aqueous electrolyte (concentration (mM), pH)	Activity measurement: Illumination[b] (irradiance (mW cm^{-2}), wavelength (nm))	H_2, μmol h^{-1}	O_2, μmol h^{-1}	Quantum yield, % (wavelength (nm))	Year[ref]
TaON	Pt (0.3)	WO_3	Pt (0.5)	NaI (5, 7)	Xe (n.r., >420)[c]	24	12	0.4 (420)	2005[151]
$CaTaO_2N$	Pt (0.3)	WO_3	Pt (0.5)	NaI (5)	Xe (n.r., >420)	~5.5	~2.5	n.r.	2008[152]
$BaTaO_2N$	*Pt (0.3)*	*WO_3*	*Pt (0.5)*	*NaI (5)*	*Xe (n.r., >420)*	*~6.5*	*~3.0*	*~0.1 (420–440)*	*2008*[152]
TaON	Pt (0.3)	TaON	RuO_2 (0.3)	NaI (1, 6)	Xe (n.r., >420)	~10	~4	0.1–0.2 (420)	2008[155]
ZrO_2–TaON	**Pt (1.0, 0.5)[d]**	**WO_3**	**Pt (0.5)**	**NaI (1.0, 0.5)[d]**	**Xe (n.r., 420–800)**	**33**	**16**	**6.3 (420.5)**	**2010**[153]
ZrO_2–TaON	Pt (1)	TiO_2–Ta_3N_5	Ir (5)	NaI (0.1)	Xe (n.r., >420)	~7	~1	n.r.	2010[156]
$SrTiO_3$:Cr,Ta	Pt (0.3)	WO_3	PtO_x (0.5)	NaI (10, 4)	Xe (n.r., >420)	32	16	1.5 (420)	2013[149]
Coumarin–$H_4Nb_6O_{17}$	Pt (0.5)	WO_3	IrO_2 (0.5) and Pt (0.5)	KI (5)	Xe (n.r., >410)	2.2	0.9	0.05 (480)	2013[164]
Carbazole–$H_4Nb_6O_{17}$	Pt (0.5)	WO_3	IrO_2 (0.5) and Pt (0.5)	KI (5)	Xe (n.r., >410)	1.7	0.7	n.r.	2013[164]
$BaTiO_3$:Rh	Pt (0.25)	WO_3	PtO_x (0.5 (Pt))	NaI (10)	Xe (n.r., >420)	1.7	0.6	0.5 (420)	2014[154]

[a] For each combination of light-absorber materials only the highest reported quantum yield (⩾0.05%) is included. Bold typeface indicates the design with the largest reported quantum yield. Italicized typeface indicates the design that absorbs at the longest wavelength. [b] Xe = 300 W xenon lamp with a Pyrex cell. [c] n.r. = not reported. [d] First value was used in H_2/O_2 activity measurement and second value was used in quantum yield measurement.

Table 5 Reports of visible-light-driven water splitting using suspensions with two particles and a non-iodine-based redox shuttle[a]

HER light absorber	HER cocatalyst (wt%)	OER light absorber	OER cocatalyst	Aqueous electrolyte (concentration (mM), pH)	Activity measurement: Illumination[b] (irradiance (mW cm^{-2}), wavelength (nm))	H_2, μmol h^{-1}	O_2, μmol h^{-1}	Quantum yield, % (wavelength (nm)) and/or STH efficiency, %	Year[ref]
$SrTiO_3$:Rh	Pt (0.5)	Bi_2MoO_6	None	$FeCl_3$ (2, 2.4 w/ H_2SO_4)	Xe (n.r., >420)	~20	~10	0.2 (440)	2004[68]
$SrTiO_3$:Rh	Pt (0.5)	WO_3	None	$FeCl_3$ (2, 2.4 w/ H_2SO_4)	Xe (n.r., >420)	~24	~11	0.5 (420)	2004[68]
$SrTiO_3$:Rh	**Ru (1)**	**$BiVO_4$**	**None**	**$FeCl_3$ (2, 2.4 w/ H_2SO_4)**	**Xe (100, >420)**	**130**	**64**	**4.2 (420), 0.1 STH**	**2013**[166]
$SrTiO_3$:Rh	Ru (0.7)	$BiVO_4$	None	$[Co(phen)_3]Cl_2$ (1, 7)	Xe (100, >420)	7.9	3.5	n.r.[c]	2013[144]
$SrTiO_3$:Rh	Ru (0.7)	TiO_2:Cr,Sb	None	$[Co(phen)_3]SO_4$ (1, 7)	Xe (100, >420)	3.0	0.8	n.r.	2013[144]
$SrTiO_3$:Rh	Ru (0.7)	$BiVO_4$	None	$[Co(bpy)_3]SO_4$ (0.5, 3.8)	Xe (100, >420)	100	47	2.1 (420), 0.06 STH	2013[144]
$SrTiO_3$:Rh	*Ru (0.5)*	*PSII*	*None*	*$Fe(CN)_6^{3-/4-}$ (5, 6)*	*Xe (250, >420)*	*~80*[d]	*~40*[d]	*n.r.*	*2014*[168]

[a] For each combination of light-absorber materials and redox shuttle only the highest reported quantum yield (≥0.1%) is included. Bold typeface indicates the design with the largest reported quantum yield and STH efficiency. Italicized typeface indicates the design that absorbs at the longest wavelength. [b] Xe = 300 W xenon lamp with a Pyrex cell. [c] n.r. = not reported. [d] Converted from mol H_2 (mol PSII)$^{-1}$ h^{-1} to μmol H_2 h^{-1} by assuming 35 chlorophyll per PSII.

particle was reported to drive overall water splitting. These particles can only be used in a Type 1 reactor, where advanced product gas separation schemes are required to prevent the existence of large volumes of explosive mixtures, and to generate pure H_2 product streams as required for ultimate use. Each of the following twelve light-absorber materials has been reported to split water when in the form of a suspension and excited by visible light with at most an applied pressure bias (*i.e.* decreased pressure): Cu_2O, $In_{1-x}Ni_xTaO_4$, $(Ga_{1-x}Zn_x)(N_{1-x}O_x)$, $(Zn_{1+x}Ge)(N_2O_x)$, Au/TiO_2, ZrO_2-modified TaON, Si/TiO_2, doped $SrTiO_3$, CoO, C_3N_4 composite, $LaMg_xTa_{1-x}O_{1+3x}N_{2-3x}$, and $CaTaO_2N$. Parameters for the best-performing systems within each materials class are displayed in chronological order in Table 2. Several recent reports of high-efficiency materials seem promising but have yet to be reproduced in the peer-reviewed literature and are either unstable on the timescale of hours or require specific protocols for continued solar PEC water-splitting activity.

Cu_2O. In 1998, the first single-particle suspension to achieve visible-light-driven PEC water splitting was reported by Domen and colleagues. The authors described Cu_2O (E_{bg} = 2.0–2.2 eV) particles in pure water that evolved stoichiometric H_2 and O_2 (by 175 hours into the experiment) when illuminated with visible light (⩾460 nm) and with an $EQY_{550-600nm} \approx 0.3\%$.[111] The system was stable over 1900 hours of continuous illumination, and isotopic labeling studies with mass spectroscopic detection suggested that O_2 evolution occurred from water, and not from decomposition of the material itself. However, follow-up studies reported that a significant fraction of the observed water-splitting activity was due to mechanochemistry introduced by the interaction of the stir bar with the Cu_2O particles and the bottom of the glass reaction vessel, termed mechanocatalytic.[112] NiO, Co_3O_4, and Fe_3O_4 were also reported to be mechanocatalytic. Later reports demonstrated that the HER took place only when no O_2 was co-evolved, and that it was accompanied by self-oxidation of the light absorber to CuO.[113] Co-evolution of H_2 and O_2 from Cu_2O are also incompatible with the limited redox stability of Cu_2O.[114]

$In_{1-x}Ni_xTaO_4$. In 2001, a suspension of monoclinic wolframite $In_{1-x}Ni_xTaO_4$ (x = 0.1; E_{bg} = 2.3 eV) particles loaded with NiO_y cocatalysts (1.0 wt%) in pure water was reported to evolve stoichiometric H_2 and O_2 when illuminated with visible light (420–540 nm) and with a $QY_{402nm} \approx 0.66\%$.[115,116] The system was reported to be stable for 400 hours of continuous illumination and with >5 turnovers per particle. RuO_2 was also used as a cocatalyst in place of NiO_y, but the performance was inferior. Recently, there is renewed interest in the basic materials parameters of this system.[117,118]

$(Ga_{1-x}Zn_x)(N_{1-x}O_x)$. In 2005, a suspension of wurtzite $(Ga_{1-x}Zn_x)(N_{1-x}O_x)$ ($x \approx 0.14$ and $E_{bg} \approx 2.7$ eV) solid-solution particles loaded with RuO_2 HER cocatalysts (5.0 wt%) in pH 3 H_2SO_4 aqueous solution was reported to evolve stoichiometric H_2 and O_2 when illuminated with visible light (≲460 nm), with a $QY_{300-480nm} \approx 0.14\%$.[119] The solid solution forms because of the similar hexagonal wurtzite lattice parameters of the individual alloyed ZnO and GaN materials. Isotopic labeling studies with mass spectroscopic detection suggested that O_2 evolution occurred from water, and not from decomposition of the material itself, and by ICP-MS, Zn was not detected in solution. In 2006, the RuO_2 HER cocatalyst was replaced by a $Rh_{2-y}Cr_yO_3$ cocatalyst and the $EQY_{420-440nm}$ increased to ~2.5%, with nearly 3 turnovers per $(Ga_{1-x}Zn_x)(N_{1-x}O_x)$ particle.[66] The amorphous Cr_2O_3 shell on the HER cocatalyst was reported to attenuate the back reaction between H_2 and O_2, due to size exclusion of O_2,[120] and allowed solar PEC water splitting to proceed with little loss in activity even under atmospheric pressure of O_2.[121] In 2008, using $(Ga_{0.82}Zn_{0.18})(N_{0.82}O_{0.18})$ particles, 2.5 wt% Rh and 2 wt% Cr, and a post-calcination step at 823 K, Domen and colleagues reported an $EQY_{420-440nm} \approx 5.9\%$, and markedly enhanced stability as evidenced by little production of N_2 (<0.12 mol% of the H_2 produced), a common degradation product of nitride materials.[122] In 2010, for the first time two cocatalysts were utilized on a single light-absorber particle to drive solar PEC water splitting, where both Rh/Cr_2O_3 core–shell HER cocatalysts and Mn_3O_4 OER cocatalysts were deposited on $(Ga_{1-x}Zn_x)(N_{1-x}O_x)$ particles, which resulted in a $QY_{>420nm} \approx 1\%$.[123] In 2012, a > 3 month stability was reported for $(Ga_{1-x}Zn_x)(N_{1-x}O_x)$ particles loaded with $Rh_{2-y}Cr_yO_3$ HER cocatalysts under continuous illumination when operated at a reduced $EQY_{400-500nm} \approx 0.16\%$, and the

suspension retained 50% of its initial activity for over half a year of continuous illumination.[81] Deactivation was ascribed to a decrease in the amount of Cr and N in the particles over time, the latter of which could be attenuated *via* initial co-loading with RuO_2 OER cocatalysts.

$(Zn_{1+x}Ge)(N_2O_x)$. In 2007, a suspension of wurtzite $(Zn_{1+x}Ge)(N_2O_x)$ (x = 0.44, $E_{bg} \approx$ 2.7 eV) solid-solution particles loaded with RuO_2 HER cocatalysts (5 wt%) in pure water was reported to evolve stoichiometric H_2 and O_2 when illuminated with visible light ($\leq$460 nm).[124] The lattice parameters of the pure materials, *i.e.* ZnO and $ZnGeN_2$, were very similar and afforded a solid solution. N_2 was detected by gas chromatography during the first five hours of illumination, but none was detected during the second five hours of illumination. Replacement of RuO_2 with a $Rh_{2-y}Cr_yO_3$ cocatalyst (3.0 wt% Rh and 0.2 wt% Cr) resulted in approximately an 8-fold increase in activity and an $EQY_{420nm} \approx$ 0.20%, and stable water-splitting activity for >50 hours of continuous illumination with no detection of N_2, a common degradation product of nitride materials.[125] In 2008, a post-calcination step at 673 K under an atmosphere of N_2 was utilized, similar to that used with $(Ga_{1-x}Zn_x)(N_{1-x}O_x)$, which resulted in a ten-fold increase in the $EQY_{420-440nm} \approx$ 2.0%.[126] The enhanced activity was attributed to a decrease in the density of surface defect states and an increase in the illumination intensity, because it was determined that the EQY did not scale linearly with the illumination intensity.

$Au/TiO_2/Al_2O_3$. In 2013, a suspension of gold nanorods electrodeposited into a porous alumina template on an ITO/TiO_2 substrate, capped with electron-beam-deposited TiO_2, and loaded with both Pt HER cocatalysts (2 nm planar equivalent) and Co-based OER cocatalysts in pH 9.6 potassium borate aqueous solution was reported to evolve stoichiometric H_2 and O_2 when illuminated with visible light from simulated solar irradiation (>410 nm; AM 1.5G, 3 Suns intensity).[127] The visible-light absorption was due to excitation of surface plasmons which resulted in $EQY_{600nm} \approx$ 0.25 and stable water-splitting activity for >60 hours of continuous illumination. The stoichiometry of H_2 and O_2 measured by gas chromatography was not strictly 2 : 1 and this imperfection was posited to be due to contamination by atmospheric O_2 during sample extraction. Although not strictly free-floating particles in solution, the demonstration of solar PEC water splitting from these Al_2O_3-confined free-floating units of approximately ten billion gold nanorods is relevant to particle suspension reactors, because each nanorod operated autonomously.

TaON. Also in 2013, a suspension of ZrO_2-modified TaON (E_{bg} = 2.5 eV) particles co-loaded with both RuO_x/Cr_2O_3 core–shell HER cocatalysts and IrO_2 OER cocatalysts in pure water was reported to evolve stoichiometric H_2 and O_2, and no N_2, when illuminated with visible light (>400 nm) and exhibited EQY_{420nm} <0.1%.[128] It was reported that the ZrO_2 modifier helped decrease the number of anionic vacancies in TaON generated during nitridation and, again, the core–shell structure of RuO_x/Cr_2O_3 attenuated reduction of O_2 due to impermeability of O_2 in the Cr_2O_3 shell.

Si/TiO_2. In 2013, a suspension of buried-junction Si nanowires (E_{bg} = 1.1 eV), fabricated by reactive-ion etching of a p-type single-crystal Si wafer followed by n^+ emitter layer formation using spin-on dopant, with part of the p-type Si core exposed and capped with Pt (by sputtering of 5–10 nm planar equivalent films) and a seed layer (by atomic-layer deposition or sputtering) for subsequent hydrothermal synthesis to form the tandem-junction TiO_2 nanowire light absorber, and loaded with Pt HER cocatalysts on Si and IrO_x OER nanoparticle cocatalysts on TiO_2 in pH 0.52 H_2SO_4 aqueous solution was reported to evolve stoichiometric H_2 and O_2 when illuminated with simulated solar irradiation (AM 1.5G, 1.5 Suns intensity).[129] The efficiency of these nanotree heterostructures was largest when 50–80% of the length of each Si nanowire was covered by TiO_2 nanowires. This system was reported to be stable for 4.5 hours and represents the first demonstration of a particle suspension containing free-floating high-aspect-ratio semiconductors, as described in Fig. 4 and Fig. 5.

$SrTiO_3$. In 2014, a suspension of Rh (0.5%) and Sb (1.0%) codoped $SrTiO_3$ (E_{bg} = 2.5 eV) particles loaded with IrO_2 (3.0 wt%) HER/OER cocatalysts in pH 3 H_2SO_4 aqueous solution was reported to evolve stoichiometric H_2 and O_2 when illuminated with visible light ($\leq$500 nm), and with an $EQY_{420nm} \approx$ 0.1%.[130] The system was reported to be stable for 21 hours of continuous illumination from a concentrated light source and with >14 turnovers per IrO_2 cocatalyst. Other cocatalysts (*i.e.* RuO_2 or Ru) were also reported to successfully evolve stoichiometric H_2 and O_2, but with a poorer efficiency.

CoO. Also in 2014, Bao and colleagues reported that a suspension of cubic CoO (E_{bg} = 2.6 eV) particles in pure water evolved H_2 and O_2 with a 5% STH efficiency when illuminated with 1 Sun AM 1.5G simulated sunlight, but the particles were unstable on the hours timescale.[131] The nanocrystals of CoO were generated using laser ablation. Isotopic labeling studies with mass spectroscopic detection suggested that O_2 evolution occurred from water, and not from decomposition of the material itself.

C_3N_4. In 2015, a carbon nitride–carbon nanodots (C_3N_4/CDots) nanocomposite ($E_{bg} \approx$ 2.76 eV) in pure water was reported by Kang, Lee, Lifshitz, and colleagues to evolve stoichiometric H_2 and O_2 *via* an H_2O_2 intermediate that rapidly disproportionated at the CDots, and exhibited an EQY_{420nm} = 16%, EQY_{600nm} = 4.42%, and a $\sim$2% STH efficiency when illuminated with 0.7–1 Suns of AM 1.5G simulated sunlight.[132] The activity persisted for up to 200 days, with no observation of CO_2 or N_2 as a reaction product, and isotopic labeling studies with mass spectroscopic detection suggested that O_2 evolution occurred from water. Interestingly, this 200 day stability was reported with regular removal and drying of the catalyst every 24 hours. However, the system was also highly stable for 45 days of continuous illumination, with no intermediate catalyst treatment and no intermediate evacuation of the evolved gases.

$LaMg_xTa_{1-x}O_{1+3x}N_{2-3x}$. Also in 2015, a suspension of perovskite $LaMg_xTa_{1-x}O_{1+3x}N_{2-3x}$ ($x = \frac{1}{3}$; $E_{bg} \approx$ 2.1 eV) solid-solution particles loaded with Rh/Cr mixed oxide (0.5 wt% Rh, 0.5 wt% Cr) HER cocatalysts in deionized water was reported to evolve stoichiometric H_2 and O_2 when illuminated with visible light ($\geq$420 nm) and with an $EQY_{440\pm30nm}$ = 0.03% and activity to 600 nm.[133] The lattice parameters of the pure

materials, *i.e.* $LaTaON_2$ and $LaMg_{2/3}Ta_{1/3}O_3$, were very similar and afforded a solid solution. Notably, a thin, amorphous hydrous $TiO_{2-m}(OH)_{2m}$ layer coated the particle–cocatalyst composites as a protective layer to prevent self-oxidation of the oxynitride to N_2. Only when coated by $TiO_{2-m}(OH)_{2m}$ was the system reported to be stable for 22 hours of continuous illumination with no N_2 detected.

$CaTaO_2N$. Also in 2015, a suspension of perovskite $CaTaO_2N$ ($E_{bg} \approx 2.43$ eV) particles loaded with $RhCrO_y$ HER cocatalysts was reported to evolve stoichiometric H_2 and O_2 when illuminated with $\geq$420 nm, and with an $EQY_{440\pm30nm} \approx 0.003\%$.[134] The same thin-layer of amorphous hydrous $TiO_{2-m}(OH)_{2m}$ was used to coat the particle–cocatalyst composites, which resulted in complete stability during 30 hours of continuous illumination with no N_2 detected.

(B) Solid-state tandem particles

This section compiles and describes reports of solar PEC water splitting using solid-state tandem-junction particles that together drive overall water splitting, akin to tandem-junction solar cells. This mechanism is often referred to as a Z-scheme due to similarities with the mechanism of natural photosynthesis. One challenge with this design is its ability to capitalize on the STH efficiency advantages of a tandem architecture which requires that sunlight be incident on the large bandgap material first. This optical condition cannot be enforced, because the particles are free to move in the suspension. In addition, these particles can also only be used in a Type 1 reactor. Parameters for the best-performing systems within each materials pair are displayed in chronological order in Table 3.

$SrTiO_3$. In 2009, the first solid-state tandem-junction particle suspension to achieve visible-light-driven PEC water splitting was reported by Kudo and colleagues.[135] The authors described Rh-doped $SrTiO_3$ (E_{bg} = 2.4 eV) HER particles loaded with Ru (1 wt%), and $BiVO_4$ (E_{bg} = 2.4 eV) OER particles which aggregated in pH 3.5 H_2SO_4 aqueous solution to form a solid-state tandem structure that evolved stoichiometric H_2 and O_2 under AM 1.5G illumination. The STH efficiency was reported to be 0.12% with an EQY_{420nm} = 1.7%, and stability over 120 hours of continuous illumination.[135,136] Photochemical reduction of graphene oxide on the particles resulted in a slight increase in the quantum yield, which was thought to arise from more rapid charge conduction between the particles.[137] Other solid-state tandem structures for solar PEC water splitting incorporating $SrTiO_3$ were also demonstrated using other visible-light-absorbing OER materials, albeit with smaller quantum yields. These included WO_3, $AgNbO_3$, Bi_2MoO_6 (E_{bg} = 2.7 eV), Cr and Sb codoped rutile TiO_2, Rh and Sb codoped rutile TiO_2,[135] and anosovite Ta_3N_5 (E_{bg} = 2.1 eV) co-loaded with CoO_x and Ir.[138] In 2014, a suspension of La and Rh codoped $SrTiO_3$ particles loaded with Ru and Ta_3N_3 particles co-loaded with CoO_x and Ir was reported to evolve stoichiometric H_2 and O_2 when illuminated with visible light (420–800 nm) and exhibited an STH efficiency of 0.037% with an EQY_{420nm} = 1.1% and stability over 12 hours of continuous illumination with no obvious N_2 formation.[139]

$ZnRh_2O_4/Ag/Ag_{1-x}SbO_{3-y}$. In 2014, a suspension of solid-state tandem particles consisting of Ag sandwiched between $ZnRh_2O_4$ and $Ag_{1-x}SbO_{3-y}$ was also reported to evolve stoichiometric H_2 and O_2 under visible-light irradiation (>500 nm) and exhibited a QY_{420nm} = 0.037%.[140] The system was reported to be stable for 144 hours of continuous illumination with no N_2 detected.

Graphene oxide. Also in 2014, a suspension of nitrogen-doped graphene-oxide quantum dots (8.1 $\pm$ 1.8 nm in diameter; $E_{bg} \approx$ 2.3 eV) in pure water was reported to evolve stoichiometric H_2 and O_2, and no N_2, when illuminated with visible light (>420 nm).[141] The metal-free slurries were stable over 3 days of continuous illumination and in comparison to a suspension of $Rh_{2-y}Cr_yO_3$/GaN:ZnO evolved H_2 and O_2 at about half the rate. It was hypothesized that a tandem pn-type photochemical diode[142] was generated between p-type and n-type domains.

(C) Tandem particles requiring a redox shuttle

This section compiles and describes reports of solar PEC water splitting using pairs of particles that are not in solid-state contact and instead require a solution redox shuttle in order to drive sustained overall water splitting. This alternative tandem design uses a redox-active electrolyte to mediate electrons between the visible-light-absorbing OER particles and visible-light-absorbing HER particles. This is the mechanism that must be utilized in Type 2 reactors and is also often termed a Z-scheme. (Note that Z-scheme mechanisms with or without a redox shuttle can also be used in Type 1 reactors.) In Type 2 reactors, solar PEC water splitting occurs by illumination of two vessels each containing a particle suspension and where one of the electronic charge carriers from each particle reacts with a redox shuttle which mediates charge exchange between the vessels. Implementation of such a design is non-trivial because redox shuttles often exhibit facile redox kinetics and thus undesired recombination reactions are often prevalent. For example, OER particles can oxidize the reduced form of the redox shuttle instead of hydroxide ions (or water), and/or HER particles can reduce the oxidized form of the redox shuttle instead of protons (or water).

Each of the following six light-absorber materials has been reported for use as HER particles in a system that split water under visible-light irradiation when in the form of a suspension, and with inclusion of OER particles and at most an applied pressure bias (*i.e.* decreased pressure): doped $SrTiO_3$, (modified) TaON, $CaTaO_2N$, $BaTaO_2N$, doped $BaTiO_3$, and dye-sensitized $H_4Nb_6O_{17}$; seven light-absorber materials/proteins have been reported that can serve as the visible-light-absorbing OER particles: (modified) WO_3, TaON, modified Ta_3N_5, $BiVO_4$, Bi_2MoO_6, doped TiO_2, and photosystem II (PSII) (Tables 4 and 5). Three general types of redox shuttle have been used with these particle combinations, *i.e.* those based on iodine (IO_3^-/I^- or I_3^-/I^-), those based on iron ($FeCl_3/FeCl_2$ or $[Fe(CN)_6]^{3-/4-}$), and those based on cobalt ($[Co(bpy)_3]SO_4$ or $[Co(phen)_3]Cl_2$). Parameters for the best-performing systems within each materials pair are displayed in chronological order in Tables 4 and 5.

For nearly all demonstrations of solar PEC water splitting only one redox state of the redox shuttle was present initially,

and thus the expected 2 : 1 stoichiometry of H_2 and O_2 was not attained at early times. Several exceptions have been reported, including the first demonstration of visible-light-driven PEC water splitting using a redox shuttle in 2001 by Arakawa and colleagues.[143] To support that the I^- did not compete with water for photogenerated holes in WO_3, Pt-loaded WO_3 particles photoelectrochemically generated O_2 in the presence of IO_3^- electron acceptor during 70 hours of continuous illumination, and at which time >96% of the initial IO_3^- had been converted to I^-. Moreover, in 2013, Kudo and workers evaluated their PEC systems in the presence of both the Co^{3+} and Co^{2+} states of their redox shuttles.[144] This was also the first report of a tandem solar PEC water-splitting demonstration using a two-vessel, Type 2 reactor design which incorporated a porous separator with pore sizes of $\sim$10 μm.[144]

Iodine-based redox shuttles. Table 4 presents, in chronological order, the best performing designs featuring an iodine-based redox shuttle. Clear and general mechanisms that elucidate the reasons for the success of iodine-based redox shuttles do not exist, but it has been suggested that single-electron-transfer recombination reactions with I_3^-, which require two electrons to generate I^-, may play a role.[145–147] This is an active area of research in the dye-sensitized solar cell community and needs more attention for application in particle suspension reactors for solar PEC water splitting, especially for the IO_3^-/I^- redox chemistry which requires that six electrons be transferred.

WO_3 OER particles. In 2001, the first particle suspension to achieve visible-light-driven PEC water splitting using a redox shuttle was reported by Arakawa and colleagues.[143] Pt-loaded (0.3 wt%), Cr (1 at%) and Ta (1 at%) codoped $SrTiO_3$ HER particles and Pt-loaded (1 wt%) WO_3 OER particles ($E_{bg} \approx$ 2.7 eV) were placed in a single vessel containing an aqueous IO_3^-/I^- redox shuttle at neutral pH and were reported to evolve stoichiometric H_2 and O_2 when illuminated with visible light (420–440 nm), with a $QY_{420.7nm} \approx 0.1\%$, and stability for over 10 days of intermittent illumination (with the light on for a total of at least 6 days).[143,148] Follow-up studies reported a $QY_{420nm} \approx 1\%$ after decreasing the concentration of electrolyte and optimizing the amount of dopants (4 at%) and the amount of OER electrocatalysts (0.5 wt%).[69] Moreover, the optimized Pt-loaded WO_3 particles evolved O_2 in the presence of up to 100 mM I^-, which is thermodynamically more favorable to oxidize than water, whereas Pt-loaded $BiVO_4$ particles did not evolve O_2 when the concentration of I^- was >10 mM. It was suggested that the activity of the Pt-loaded WO_3 particles in the presence of iodide was due in part to preferential adsorption of the IO_3^- electron acceptor on Pt-loaded WO_3. In 2013, an EQY_{420nm} = 1.5% was reported using pH 4 conditions and PtO_x-loaded (0.5 wt%) WO_3 OER particles that had been impregnated with Cs^+ at 773 K and then ion-exchanged with H^+ to generate "ion-exchangeable site[s]".[149,150]

In 2005, the doped $SrTiO_3$ particles were replaced with TaON HER particles (E_{bg} = 2.5 eV) with the same Pt loading, and the system was reported to be stable for 100 hours of continuous illumination with no N_2 detected and an $EQY_{420nm} \approx 0.4\%$.[151] In 2008, the wavelength onset for H_2 evolution for PEC water splitting was extended to 510 nm using $CaTaO_2N$ HER particles with the same Pt loading, and to 660 nm using $BaTaO_2N$ HER particles with the same Pt loading, but with a decreased $EQY_{420–440nm} \approx 0.1\%$ (in conjunction with the same Pt-loaded WO_3 OER particles) and some initial N_2 evolution.[152] In 2010, Domen and colleagues reported Pt-loaded (0.5 wt%) ZrO_2-modified TaON (9.1 at% ZrO_2) (E_{bg} = 2.2 eV) HER particles that resulted in an $EQY_{420.5nm}$ that increased by over an order-of-magnitude to 6.3% (in conjunction with the same Pt-loaded WO_3 OER particles).[153] In 2014, a suspension of Pt-loaded (0.25 wt%), Rh-doped (1.0 mol%) perovskite $BaTiO_3$ HER particles and PtO_x-loaded (0.5 wt% Pt) WO_3 OER particles was reported to evolve stoichiometric H_2 and O_2 when illuminated with visible light (>420 nm) and was stable for 30 hours of continuous illumination.[154]

Tantalum–nitride OER particles. Particles that perform the OER and absorb more visible light than WO_3 are also actively being investigated. In 2008, a suspension of Pt-loaded (0.3 wt%) TaON HER particles and RuO_2-loaded (0.3 wt%) TaON OER particles was reported to evolve stoichiometric H_2 and O_2 when illuminated with visible light, and with only a small amount of initial N_2 evolution.[155] The initial $EQY_{420nm} \approx 0.1–0.2\%$ was smaller than that observed using WO_3 even though TaON absorbed more visible light. In 2010, a suspension of Pt-loaded (1 wt%) ZrO_2-modified TaON HER particles and Ta_3N_5 (E_{bg} = 2.1 eV) OER particles modified with Ir (5 wt%) and rutile TiO_2 was reported to evolve H_2 and O_2 for 60 hours when continuously illuminated with visible light (>420 nm).[156]

Molecular dyes on oxide particles. Molecular dye light absorbers have been used to drive solar PEC water splitting.[96,157–159] In 1980, Grätzel and colleagues reported the first successful use of dye sensitizers to impart PEC water splitting using visible light (>450 nm), with Ru–polypyridyl dyes anchored to TiO_2 particles co-loaded with Pt and RuO_2 cocatalysts.[158] The reported stoichiometry of H_2 and O_2 often deviated from the ideal 2 : 1 v/v ratio, and other studies indicated that reduction of adsorbed O_2 may have been the cause of the reduced O_2 stoichiometry.[80,160–162] In 2009, an aqueous suspension of Pt-loaded (0.5 wt%) $H_4Nb_6O_{17}$ HER particles with anchored coumarin organic dyes as sensitizers, WO_3 OER particles co-loaded with IrO_2 (0.5 wt%) and Pt (0.5 wt%), and the I_3^-/I^- redox shuttle was reported to evolve approximately stoichiometric H_2 and O_2 when illuminated with visible light (>400 nm).[163] The system was stable for 48 hours of illumination, where it exhibited >200 turnovers per dye; however, the rate of water splitting was limited by the low $QY_{500nm} < 0.1\%$ for dye-sensitized H_2 evolution. Insertion of an oligothiophene moiety between the donor and acceptor part of coumarin or carbazole dyes was reported to significantly improve the stability of the dye sensitizers in aqueous electrolytes, resulting in stability for 64 hours of continuous illumination and a maximum of >500 turnovers per dye for a coumarin dye containing two thiophenes rings.[164]

Iron-based redox shuttles. Iodate/iodide redox chemistry is somewhat irreversible due to the plethora of iodine oxide intermediates that can be formed during oxidation of iodide (I^-) from the 1− to 5+ oxidation state, as IO_3^-. Thus, other redox shuttles may be of practical interest. Toward this, in

2004, Kudo and colleagues used a chloride salt of the $Fe^{3+/2+}$ redox shuttle in pH 2.4 aqueous electrolyte containing Pt-loaded (0.5 wt%), Rh-doped (1 at%) $SrTiO_3$ HER particles and $BiVO_4$, WO_3, or Bi_2MoO_6 OER particles to impart H_2 and O_2 evolution when illuminated with visible light (>420 nm).[68,70] EQY_{440nm} = 0.3%, 0.2%, and 0.2% was reported for each system, respectively, as well as stability for 120 hours, 158 hours, and 22 hours of continuous illumination, and multiple turnovers per Fe^{3+} in each case. Only systems with either WO_3 or $BiVO_4$ were reported to produce stoichiometric H_2 and O_2 with EQY_{420nm} = 0.5% and 0.4%, respectively. The pH was adjusted with H_2SO_4 and the experimental pH value was chosen to prevent formation of iron oxide colloids. Although reduction of Fe^{3+} at Pt is a recombination mechanism, as the concentration of Fe^{3+} increased, the rate of H_2 evolution also increased. It was suggested that, akin to IO_3^-, the proposed Fe^{3+} species ($[Fe^{III}(SO_4)(H_2O)_5]^+$ and $[Fe^{III}(OH)(H_2O)_5]^{2+}$) adsorbed onto Pt and suppressed the undesired H_2 + Fe^{3+} recombination reaction that is typically catalyzed at Pt.

In 2008, the Pt HER cocatalysts were replaced with Ru (0.7 wt%) and when mixed with $BiVO_4$ OER particles an EQY_{420nm} = 0.3% was reported for stoichiometric H_2 and O_2 evolution when illuminated with visible light (>420 nm).[165] Moreover, the reported activity did not depend on the amount of evolved H_2 and O_2 in the headspace during 70 hours of continuous evolution of gases, whereas when Pt HER cocatalysts were used decreased activity was apparent by 20 hours. $Fe^{3+/2+}$-mediated recombination reactions under pressurized H_2 or O_2 were reported to be slower at the oxidized Ru cocatalysts than at previously reported metallic Pt cocatalysts. Pt activity was returned upon releasing the built-up H_2 and O_2 pressure. In 2013, an EQY_{420nm} = 4.2% and a 0.1% STH efficiency for stoichiometric H_2 and O_2 evolution were reported for these materials when the HER particles were synthesized by a new procedure and illuminated with 1 Sun AM 1.5G simulated sunlight. The optimal procedure included excess Sr, 2 at% Rh dopant, and 1 wt% Ru HER cocatalysts.[166] In 2014, these $SrTiO_3$ HER particles were combined with Rh (1.0%) and Sb (1.0%) codoped $SrTiO_3$ particles loaded with IrO_x (3.0 wt%) OER cocatalysts to demonstrate stable H_2 and O_2 evolution for 90 hours of continuous illumination.[167]

Also in 2014, Li, Chen, and colleagues reported a hybrid suspension consisting of photosystem II, an $[Fe(CN)_6]^{3-/4-}$ redox shuttle, and Ru-loaded (0.5 wt%) $SrTiO_3$:Rh or Ru_2S_3-loaded (0.2 wt%) hexagonal CdS dispersed in a sodium phosphate buffer solution (pH 6.0 or pH 7.0) that evolved near stoichiometric H_2 and O_2 when illuminated with visible light (>420 nm).[168] The $SrTiO_3$ system at pH 7.0 was reported to be the most efficient with approximately stoichiometric gas evolution, >3700 turnovers per PSII, and an activity of $\sim$2500 mol H_2 (mol PSII)$^{-1}$ h^{-1}, which corresponds to $\sim$80 μmol H_2 h^{-1}, when assuming 35 chlorophyll per PSII.[169]

Cobalt-based redox shuttles. Historically, efficient dye-sensitized solar cells use iodine-based redox electrolytes in nitrile solvents to mediate charge transport from metal-oxide nanoparticles, because recombination from the metal-oxide nanoparticles is much slower than with most other redox shuttles.[146] Alternative redox shuttles consisting of inorganic coordination compounds based on cobalt tris(bipyridine), which absorb much less visible light than I_3^-, have also been used in efficient dye-sensitized solar cells,[170] including the state-of-the-art demonstration.[171] In 2013, Kudo and colleagues used homoleptic $Co^{3+/2+}$ polypyridyl coordination compounds as the redox shuttle in particle suspensions for solar PEC water splitting.[144] Ru-loaded (0.7 wt%), Rh-doped (1 at%) $SrTiO_3$ HER particles and OER particles consisting of $BiVO_4$, WO_3, or Cr (2.3%) and Sb (3.45%) codoped TiO_2 were reported to evolve H_2 and O_2 when illuminated with visible light (>420 nm). The WO_3 OER particles were reported to exhibit $QY_{\geq 420nm}$ = 0.1%, while the $BiVO_4$ OER particles reached a maximum QY_{420nm} = 2.1% (0.06% STH efficiency), and evolved the gases in an approximately 2 : 1 stoichiometry for >100 hours of continuous illumination, when the particles were prepared using 3% excess Sr (to Ti + Rh) and were evaluated at pH 3.8 with 0.5 mM redox shuttle (0.2 mM for STH measurement). Each particle was evaluated in the presence of redox shuttle molecules in just one redox state or equimolar concentrations of molecules in both redox states. Comparing the case with only one redox state present *versus* both, the Rh-doped $SrTiO_3$ HER particles lost only 6% (bpy ligands, pH 6.8), 14% (bpy ligands, pH 3.8), and 23% (phen ligands, pH 6.8) of initial activity, while the $BiVO_4$ OER particles lost 23% (bpy ligands, pH 6.8), 87% (bpy ligands, pH 3.8), and 71% (phen ligands, pH 6.8) of initial activity (bpy is 2,2′-bipyridine and phen is 1,10-phenanthroline). In addition, this was the first report where an electrochemical cell with two vessels separated by a membrane was used, which strongly resembled a Type 2 reactor design and exhibited an initial $QY_{\geq 420nm} \approx$ 0.05% under sunlight illumination in autumn in Tokyo.[144]

VI. Conclusions

Solar water splitting could supply clean, renewable fuel for our civilization, assuming an inexpensive, efficient, and stable reactor is realized. PEC reactors based on particle suspensions, *i.e.* Type 1 and Type 2 reactors, have low projected levelized costs of H_2 and are projected to be cost-competitive with gasoline sold in the U.S. even at only single-digit STH conversion efficiencies. However, many challenges remain before these reactors become commercial realities. At least twenty different light-absorber materials have demonstrated solar PEC water splitting using either a single particle or solid-state tandem particle in a Type 1 reactor design, as well as particles and redox shuttles that would be suitable for a Type 2 reactor design. Two *STH efficiencies* were reported that exceeded 1%: a CoO suspension that exhibited a 5% STH efficiency but was only stable on the timescale of hours, and a carbon nitride–carbon nanodots composite that demonstrated a $\sim$2% STH efficiency and 200 days of operation, with daily particle removal and drying. In lieu of these unsustainable demonstrations, all other reported *quantum yields* were <7%, which is over an order-of-magnitude smaller than the values reported for state-of-the-art fixed electrodes.[172] In other words,

efficient, stable, inexpensive, and proven particles for solar PEC water splitting that can be used as suspensions in these reactors *do not yet exist*. Only through continued funding and research into particle materials and reactors for solar PEC water splitting will these technologies one day constitute an affordable and practical option for centralized renewable H_2 generation from water. In conclusion, big-picture target research goals for those interested in particle suspension reactors for solar PEC water splitting are presented below.

- Fabricate particle suspensions that are able to split water under 1 Sun of AM 1.5G illumination against pressures of 1 bar H_2 and 1 bar O_2. For Z-scheme mechanisms involving a redox shuttle, also include both halves of the redox shuttle.
- Engineer and evaluate separation processes (Type 1 reactors) and separator materials (Type 2 reactors).
- Through numerical modeling and simulation, determine which reactor design, vessel arrangement, vessel dimensions, *etc.* and which particle size, shape, concentration, *etc.* satisfy chemical engineering demands.
- Perform techno-economic cost analyses for plausible alternative piping designs, flow schemes, and product separation technologies, and assess their applicability computationally.
- Computationally model and perform techno-economic cost analyses on the active materials (*e.g.* particles, cocatalysts, redox shuttles, separators), in order to optimize the selection and fabrication of future improved materials.
- Fabricate particles and cocatalysts that are most amenable to the reactor design constraints and result in the most efficient, robust, inexpensive, and scalable reactors, and evaluate entire prototype reactors under solar illumination conditions.

Appendix

For a sustainable and safe Type 1 reactor, the H_2 and O_2 reaction products from the water-splitting reactions must be separated to at least beyond the flammable limits, where the lower limit is 4% H_2 in O_2.[20] The energy loss due to isothermally separating H_2 from an ideal 2 : 1 v/v stoichiometric H_2/O_2 reaction product mixture can be estimated to be 8.7% of the energy stored in H_2, per the following calculation: the H_2/O_2 gas mixture inside (in) the water-splitting reactor vessel has initial mole fractions of H_2 and O_2 of $X(H_2, in) = \frac{2}{3}$ (0.667) and $X(O_2, in) = \frac{1}{3}$ (0.333). Then, it is assumed that an H_2-selective membrane puts this mixture into diffusional equilibrium with pure H_2 outside (out) the reactor vessel, in a storage tank at a pressure of 1 bar. For equilibrium to hold between the reactor vessel and the storage tank, the partial pressures of H_2 inside and outside the reactor vessel must be equal, *i.e.* $p(H_2, in) = p(H_2, out) = 1$ bar. After pressurization and equilibration due to H_2 diffusion, this requires that the total pressure inside the reactor vessel be 25 bar (*i.e.* 1 bar H_2 (4%) and 24 bar O_2 (96%)), according to eqn (3),

$$X(H_2, in) \times p(tot, in) = X(H_2, out) \times p(tot, out) \quad (3a)$$

$$p(tot, in)_{final} = X(H_2, out) \times p(tot, out)/X(H_2, in)_{final}$$

$$p(tot, in)_{final} = (1.0 \times 1 \text{ bar})/0.04 = 25 \text{ bar} \quad (3b)$$

Because the partial pressure of O_2 in the pressurized gas mixture does not change during H_2 diffusion, the initial 2 : 1 v/v stoichiometric H_2/O_2 mixture at 1 bar must be pressurized to 72 bar prior to H_2 diffusion out of the reactor vessel. This assumes a one-step reversible and isothermal pressurization process (in a closed system) and is calculated using eqn (4),

$$p(tot, in)_{initial} = (\nu_{H_2} + \nu_{O_2}) \times p(O_2, in)$$

$$p(tot, in)_{initial} = (2 + 1) \times 24 \text{ bar} = 72 \text{ bar} \quad (4)$$

The pV work required to pressurize the initial H_2/O_2 mixture from 1 bar to 72 bar is 10.6 kJ mol^{-1}. Again, this assumes a one-step reversible and isothermal pressurization process (in a closed system) and is calculated using the equation for the differential Gibbs free energy and the ideal gas law at 25 °C, according to eqn (5),

$$\Delta G = nRT \ln(p_2/p_1)$$

$$\Delta G = 2479 \ln(72 \text{ bar}/1 \text{ bar}) = 10.6 \text{ kJ per mole of initial products} \quad (5)$$

This equals 6.7% of the free energy content in the initial 1 mole of gas mixture (*i.e.* 0.667 × 237 kJ mol^{-1} = 158 kJ mol^{-1}). This brief estimate shows that overall the STH efficiency is reduced by ~8.7% for this type of gas separation (6.7% pressurization energy loss plus 2% H_2 energy loss due to the residual 4% H_2 remaining in the vessel).

Acknowledgements

The authors thank Dr. Eric Miller for the inspiration to compile this review, and the members of the U.S. Department of Energy's Photoelectrochemical Working Group and Task 35 (Renewable Hydrogen) of the International Energy Agency's Hydrogen Implementing Agreement for helpful comments, suggestions, and discussions, specifically Prof. Ryu Abe (Kyoto University), Prof. Jason Baxter (Drexel University), Prof. Jiming Bao (University of Houston), Prof. Dan Esposito (Columbia University), Dr. Arnold Forman (Bio-Logic), Prof. Sophia Haussener (École polytechnique fédérale de Lausanne), Prof. Akihiko Kudo (Tokyo University of Science), Dr. Kazuhiko Maeda (Tokyo Institute of Technology), Dr. Sixto Malato (Plataforma Solar de Almería), Dr. Steve Reece (Sun Catalytix), and Prof. Wilson Smith (Delft University of Technology). D.M.F. acknowledges support by the National Science Foundation Graduate Research Fellowship under Grant No. DGE-1321846. This material is based upon work performed by the Joint Center for Artificial Photosynthesis, a DOE Energy Innovation Hub, as follows: work by S.H. and F.A.H. was supported through the Office of Science of the U.S. Department of Energy under Award No. DE-SC0004993. N.S. is supported by the University of California Santa Barbara Air Products Fellowship and by the National Science Foundation (EFRI-1038234). T.H. and K.D. acknowledge financial support *via* a Grant-in-Aids for Specially Promoted Research (no. 23000009) of the Japan Society for the Promotion of Science (JSPS). F.E.O. thanks Research Corporation for Science

Advancement for a Scialog award and the National Science Foundation under CHE – 1152250 and CBET 1133099. Any opinions, findings, conclusions, or recommendations expressed in this material are those of the author and do not necessarily reflect the views of the National Science Foundation. S.A. acknowledges support from the Department of Chemistry and the School of Physical Sciences at the University of California Irvine and the U.S. Department of Energy under Award No. DE-EE0006963. A summary version of this review paper (DOI: 10.2172/1179198), and associated summary tables that will be updated as the field progresses, will be available on the working group website (http://energy.gov/eere/fuelcells/photoelectrochemical-working-group).

References

1 A. Bard and M. A. Fox, *Acc. Chem. Res.*, 1995, **28**, 141–145.
2 B. D. James, G. N. Baum, J. Perez, K. N. Baum, *DOE Contract Number GS-10F-009J*, 2009, 1–128.
3 B. A. Pinaud, J. D. Benck, L. C. Seitz, A. J. Forman, Z. Chen, T. G. Deutsch, B. D. James, K. N. Baum, G. N. Baum, S. Ardo, H. Wang, E. Miller and T. F. Jaramillo, *Energy Environ. Sci.*, 2013, **6**, 1983–2002.
4 J. R. Bolton, S. J. Strickler and J. S. Connolly, *Nature*, 1985, **316**, 495–500.
5 M. F. Weber and M. J. Dignam, *J. Electrochem. Soc.*, 1984, **131**, 1258–1265.
6 S. Hu, C. Xiang, S. Haussener, A. D. Berger and N. S. Lewis, *Energy Environ. Sci.*, 2013, **6**, 2984–2993.
7 L. C. Seitz, Z. Chen, A. J. Forman, B. A. Pinaud, J. D. Benck and T. F. Jaramillo, *ChemSusChem*, 2014, **7**, 1372–1385.
8 H. Döscher, J. Geisz, T. Deutsch and J. Turner, *Energy Environ. Sci.*, 2014, **7**, 2951–2956.
9 S. Licht, B. Wang, S. Mukerji, T. Soga, M. Umeno and H. Tributsch, *Int. J. Hydrogen Energy*, 2001, **26**, 653–659.
10 J. W. Ager III, M. Shaner, K. Walczak, I. D. Sharp and S. Ardo, *Energy Environ. Sci.*, 2015, DOI: 10.1039/C5EE00457H.
11 S. E. Braslavsky, *Pure Appl. Chem.*, 2007, **79**, 293–465.
12 K. Maeda and K. Domen, *J. Phys. Chem. Lett.*, 2010, **1**, 2655–2661.
13 A. Agiral, H. Sen Soo and H. Frei, *Chem. Mater.*, 2013, **25**, 2264–2273.
14 S. Y. Reece, Sun Catalytix, Cambridge, MA, Personal communication, 2012.
15 S. Kumar, A. K. Panda and R. K. Singh, *Resour., Conserv. Recycl.*, 2011, **55**, 893–910.
16 B. D. James, G. N. Baum, J. Perez, K. N. Baum, *DOE Contract Number SR-560*-46674, 2009, 1–193.
17 C. Vasile and M. Pascu, *Practical Guide to Polyethylene*, RAPRA Technology, Shrewsbury, 2005.
18 D. M. Blake, C. Kennedy, *DOE Hydrogen Program*, 2005, 236–240.
19 Berry Plastics, Agricultural Film, http://www.berryplastics.com/products/protection-solutions/agricultural-film, accessed Apr 5, 2015.
20 N. Cohen, Aerospace Report No. TR-92(2534)-11992, 1–25.
21 A. J. Bard and L. R. Faulkner, *Electrochemical Methods: Fundamentals and Applications*, John Wiley & Sons, Inc., New York, 2nd edn, 2001.
22 J. O. Bockris and A. K. N. Reddy, *Modern Electrochemistry*, Kluwer Academic Publishers, New York, 2nd edn, 1998, vol. 1.
23 R. Abe, K. Sayama, K. Domen and H. Arakawa, *Chem. Phys. Lett.*, 2001, **344**, 339–344.
24 W. Gaieck and S. Ardo, *Rev. Adv. Sci. Eng.*, 2014, **3**, 277–287.
25 K. A. Mauritz and R. B. Moore, *Chem. Rev.*, 2004, **104**, 4535–4586.
26 F. Lufrano, V. Baglio, P. Staiti, V. Antonucci and A. S. Arico, *J. Power Sources*, 2013, **243**, 519–534.
27 W. Hinsberg and F. Houle, *J. Vac. Sci. Technol., B: Microelectron. Nanometer Struct.–Process., Meas., Phenom.*, 2005, **23**, 2427–2435.
28 J. M. Foley, M. J. Price, J. I. Feldblyum and S. Maldonado, *Energy Environ. Sci.*, 2012, **5**, 5203–5220.
29 M. J. Naughton, K. Kempa, Z. F. Ren, Y. Gao, J. Rybczynski, N. Argenti, W. Gao, Y. Wang, Y. Peng, J. R. Naughton, G. McMahon, T. Paudel, Y. C. Lan, M. J. Burns, A. Shepard, M. Clary, C. Ballif, F. J. Haug, T. Söderström, O. Cubero and C. Eminian, *Phys. Status Solidi RRL*, 2010, **4**, 181–183.
30 J. D. Christesen, X. Zhang, C. W. Pinion, T. A. Celano, C. J. Flynn and J. F. Cahoon, *Nano Lett.*, 2012, **12**, 6024–6029.
31 T. J. Kempa, J. F. Cahoon, S.-K. Kim, R. W. Day, D. C. Bell, H.-G. Park and C. M. Lieber, *Proc. Natl. Acad. Sci. U. S. A.*, 2012, **109**, 1407–1412.
32 W. A. Smith, I. D. Sharp, N. Strandwitz and J. Bisquert, *Energy Environ. Sci.*, 2015, DOI: 10.1039/C5EE01822F.
33 S. J. Fonash, *Solar Cell Device Physics*, Elsevier Academic Press, Amsterdam, 2nd edn, 2010.
34 G. Hodes, I. D. J. Howell and L. M. Peter, *J. Electrochem. Soc.*, 1992, **139**, 3136–3140.
35 A. Fitch, N. C. Strandwitz, B. S. Brunschwig and N. S. Lewis, *J. Phys. Chem. C*, 2013, **117**, 2008–2015.
36 B. M. Kayes, H. A. Atwater and N. S. Lewis, *J. Appl. Phys.*, 2005, **97**, 114302.
37 S. Hu, C.-Y. Chi, K. T. Fountaine, M. Yao, H. A. Atwater, P. D. Dapkus, N. S. Lewis and C. Zhou, *Energy Environ. Sci.*, 2013, **6**, 1879–1890.
38 M. D. Kelzenberg, S. W. Boettcher, J. A. Petykiewicz, D. B. Turner-Evans, M. C. Putnam, E. L. Warren, J. M. Spurgeon, R. M. Briggs, N. S. Lewis and H. A. Atwater, *Nat. Mater.*, 2010, **9**, 239–244.
39 P. Würfel, *Physics of Solar Cells: From Principles to New Concepts*, Wiley, Weinheim, 2005.
40 F. E. Osterloh, *J. Phys. Chem. Lett.*, 2014, **5**, 2510–2511.
41 M. D. Kelzenberg, D. B. Turner-Evans, M. C. Putnam, S. W. Boettcher, R. M. Briggs, J. Y. Baek, N. S. Lewis and H. A. Atwater, *Energy Environ. Sci.*, 2011, **4**, 866–871.
42 R. A. Street, W. S. Wong and C. Paulson, *Nano Lett.*, 2009, **9**, 3494–3497.
43 A. Kumar, P. G. Santangelo and N. S. Lewis, *J. Phys. Chem.*, 1992, **96**, 834–842.

44 C. McCrory, S. Jung, J. C. Peters and T. F. Jaramillo, *J. Am. Chem. Soc.*, 2013, **135**, 16977–16987.
45 C. C. L. McCrory, S. Jung, I. M. Ferrer, S. Chatman, J. C. Peters and T. F. Jaramillo, *J. Am. Chem. Soc.*, 2015, **137**, 4347–4357.
46 T. Hisatomi, K. Takanabe and K. Domen, *Catal. Lett.*, 2015, **145**, 95–108.
47 W. B. Russel, D. A. Saville and W. R. Schowalter, *Colloidal Dispersions*, Cambridge Unviersity Press, Cambridge, 1992.
48 F. Jin, J. Li, X. Ye and C. Wu, *J. Phys. Chem. B*, 2007, **111**, 11745–11749.
49 B. Derjaguin and L. Landau, *Prog. Surf. Sci.*, 1993, **43**, 30–59.
50 E. J. W. Verwey and J. T. G. Overbeek, *Theory of the Stability of Lyophobic Colloids*, Elsevier, New York, 1948.
51 K. Maeda and K. Domen, *J. Phys. Chem. C*, 2007, **111**, 7851–7861.
52 A. Kudo and Y. Miseki, *Chem. Soc. Rev.*, 2009, **38**, 253–278.
53 F. E. Osterloh, *Chem. Soc. Rev.*, 2013, **42**, 2294–2320.
54 F. E. Osterloh, *Chem. Mater.*, 2008, **20**, 35–54.
55 H. Yoneyama, *Crit. Rev. Solid State Mater. Sci.*, 1993, **18**, 69–111.
56 T. Bak, J. Nowotny, M. Rekas and C. Sorrell, *Int. J. Hydrogen Energy*, 2002, **27**, 991–1022.
57 A. Kudo, *Int. J. Hydrogen Energy*, 2007, **32**, 2673–2678.
58 X. Chen, S. Shen, L. Guo and S. S. Mao, *Chem. Rev.*, 2010, **110**, 6503–6570.
59 A. A. Ismail and D. W. Bahnemann, *Sol. Energy Mater. Sol. Cells*, 2014, **128**, 85–101.
60 K. Domen, S. Naito, T. Onishi and K. Tamaru, *Chem. Phys.*, 1982, **92**, 433–434.
61 R. Li, F. Zhang, D. Wang, J. Yang, M. Li, J. Zhu, X. Zhou, H. Han and C. Li, *Nat. Commun.*, 2013, **4**, 1432.
62 P. A. Morris Hotsenpiller, J. D. Bolt, W. E. Farneth, J. B. Lowekamp and G. S. Rohrer, *J. Phys. Chem. B*, 1998, **102**, 3216–3226.
63 C. G. Read, E. M. P. Steinmiller and K. S. Choi, *J. Am. Chem. Soc.*, 2009, **131**, 12040–12041.
64 S. E. Habas, P. Yang and T. Mokari, *J. Am. Chem. Soc.*, 2008, **130**, 3294–3295.
65 L. Amirav and A. P. Alivisatos, *J. Phys. Chem. Lett.*, 2010, **1**, 1051–1054.
66 K. Maeda, K. Teramura, D. Lu, T. Takata, N. Saito, Y. Inoue and K. Domen, *Nature*, 2006, **440**, 295.
67 K. Fujihara, T. Ohno and M. Matsumura, *J. Chem. Soc., Faraday Trans.*, 1998, **94**, 3705–3709.
68 H. Kato, M. Hori, R. Konta, Y. Shimodaira and A. Kudo, *Chem. Lett.*, 2004, **33**, 1348–1349.
69 R. Abe, K. Sayama and H. Sugihara, *J. Phys. Chem. B*, 2005, **109**, 16052–16061.
70 H. Kato, Y. Sasaki, A. Iwase and A. Kudo, *Bull. Chem. Soc. Jpn.*, 2007, **80**, 2457–2464.
71 Z. Chen, T. F. Jaramillo, T. G. Deutsch, A. Kleiman-Shwarsctein, A. J. Forman, N. Gaillard, R. Garland, K. Takanabe, C. Heske, M. Sunkara, E. W. McFarland, K. Domen, E. L. Miller, J. A. Turner and H. N. Dinh, *J. Mater. Res.*, 2010, **25**, 3–16.
72 R. H. Coridan, A. C. Nielander, S. A. Francis, M. T. McDowell, V. Dix, S. M. Chatman and N. Lewis, *Energy Environ. Sci.*, 2015, DOI: 10.1039/C5EE00777A.
73 W. Shockley and H. J. Queisser, *J. Appl. Phys.*, 1961, **32**, 510–519.
74 R. Rocheleau and E. L. Miller, *Int. J. Hydrogen Energy*, 1997, **22**, 771–782.
75 N. Lewis, *Electrochem. Soc. Interface*, 2013, **22**, 43–49.
76 H. G. Kim, D. W. Hwang and J. S. Lee, *J. Am. Chem. Soc.*, 2004, **126**, 8912–8913.
77 H. G. Kim, O. S. Becker, J. S. Jang, S. M. Ji, P. H. Borse and J. S. Lee, *J. Solid State Chem.*, 2006, **179**, 1214–1218.
78 A. Ishikawa, T. Takata, T. Matsumura, J. N. Kondo, M. Hara, H. Kobayashi and K. Domen, *J. Phys. Chem. B*, 2004, **108**, 2637–2642.
79 H. Dürr, S. Boßmann and A. Beuerlein, *J. Photochem. Photobiol., A*, 1993, **73**, 233–245.
80 A. Mills and G. Porter, *J. Chem. Soc., Faraday Trans. 1*, 1982, **78**, 3659–3669.
81 T. Ohno, L. Bai, T. Hisatomi, K. Maeda and K. Domen, *J. Am. Chem. Soc.*, 2012, **134**, 8254–8259.
82 M. R. Shaner, K. T. Fountaine, S. Ardo, R. H. Coridan, H. A. Atwater and N. S. Lewis, *Energy Environ. Sci.*, 2014, **7**, 779–790.
83 Z. Chen, H. N. Dinh and E. Miller, *Photoelectrochemical Water Splitting Standards, Experimental Methods, and Protocols*, Springer, New York, 2013.
84 J. Zhao and F. E. Osterloh, *J. Phys. Chem. Lett.*, 2014, **5**, 782–786.
85 M. R. Waller, T. K. Townsend, J. Zhao, E. M. Sabio, R. L. Chamousis, N. D. Browning and F. E. Osterloh, *Chem. Mater.*, 2012, **24**, 698–704.
86 T. K. Townsend, N. D. Browning and F. E. Osterloh, *Energy Environ. Sci.*, 2012, **5**, 9543–9550.
87 I. Mora-Seró, J. Bisquert, T. Dittrich, A. Belaidi, A. S. Susha and A. L. Rogach, *J. Phys. Chem. C*, 2007, **111**, 14889–14892.
88 D. V. Esposito, J. B. Baxter, J. John, N. Lewis, T. P. Moffat, T. Ogitsu, G. D. O'Neil, T. A. Pham, A. A. Talin, J. M. Velazquez and B. Wood, *Energy Environ. Sci.*, 2015, DOI: 10.1039/C5EE00835B.
89 T. K. Townsend, N. D. Browning and F. E. Osterloh, *ACS Nano*, 2012, **6**, 7420–7426.
90 W. H. Brattain and C. G. B. Garrett, *Bell Syst. Tech. J.*, 1955, **34**, 129–176.
91 H. Gerischer, *Annu. Rev. Phys. Chem.*, 1960, **12**, 227–254.
92 H. Lewerenz and L. Peter, *Photoelectrochemical Water Splitting: Materials, Processes and Architectures*, The Royal Society of Chemistry, Cambridge, 2013.
93 G. N. Schrauzer and T. D. Guth, *J. Am. Chem. Soc.*, 1977, **99**, 7189–7193.
94 H. Van Damme and W. K. Hall, *J. Am. Chem. Soc.*, 1979, **101**, 4373–4374.
95 T. Kawai and T. Sakata, *Chem. Phys. Lett.*, 1980, **72**, 87–89.
96 K. Kalyanasundaram and M. Grätzel, *Angew. Chem., Int. Ed. Engl.*, 1979, **18**, 701–702.

97 K. Kalyanasundaram, E. Borgarello, D. Duonghong and M. Grätzel, *Angew. Chem., Int. Ed. Engl.*, 1981, **11**, 987–988.
98 J. Lehn, J. P. Sauvage and R. Ziessel, *Nouv. J. Chim.*, 1980, **4**, 623–627.
99 K. Domen, S. Naito, M. Soma, T. Onishi and K. Tamaru, *J. Chem. Soc., Chem. Commun.*, 1980, 543–544.
100 S. Sato and J. M. White, *Nippon Kagaku Kaishi*, 1988, **72**, 1182–1187.
101 R. Abe, *J. Photochem. Photobiol., C*, 2010, **11**, 179–209.
102 K. Rajeshwar, *J. Appl. Electrochem.*, 2007, **37**, 765–787.
103 S. Haussener, C. Xiang, J. M. Spurgeon, S. Ardo, N. S. Lewis and A. Z. Weber, *Energy Environ. Sci.*, 2012, **5**, 9922–9935.
104 M. A. Green, K. Emery, Y. Hishikawa, W. Warta and E. D. Dunlop, *Prog. Photovolt.: Res. Appl.*, 2014, **22**, 701–710.
105 T. Hisatomi, J. Kubota and K. Domen, *Chem. Soc. Rev.*, 2014, **43**, 7520–7535.
106 S. Chen and L. Wang, *Chem. Mater.*, 2012, **24**, 3659–3666.
107 L. Sang, Y. Zhao and C. Burda, *Chem. Rev.*, 2014, **114**, 9283–9318.
108 J. Sato, N. Saito, Y. Yamada, K. Maeda, T. Takata, J. N. Kondo, M. Hara, H. Kobayashi, K. Domen and Y. Inoue, *J. Am. Chem. Soc.*, 2005, **127**, 4150–4151.
109 K. Tennakone, R. Tantrigoda, S. Abeysinghe, S. Punchihewa and C. A. N. Fernando, *J. Photochem. Photobiol., A*, 1990, **52**, 43–46.
110 K. Sayama, R. Yoshida, H. Kusama, K. Okabe, Y. Abe and H. Arakawa, *Chem. Phys. Lett.*, 1997, **277**, 387–391.
111 M. Hara, T. Kondo, M. Komoda, S. Ikeda, J. N. Kondo, K. Domen, M. Hara, K. Shinohara and A. Tanaka, *Chem. Commun.*, 1998, 357–358.
112 S. Ikeda, T. Takata, T. Kondo, G. Hitoki, M. Hara, J. N. Kondo, K. Domen, H. Hosono, H. Kawazoe and A. Tanaka, *Chem. Commun.*, 1998, 2185–2186.
113 S. Kakuta and T. Abe, *Electrochem. Solid-State Lett.*, 2009, **12**, P1–P3.
114 P. E. De Jongh, D. Vanmaekelbergh and J. J. Kelly, *Chem. Commun.*, 1999, 1069–1070.
115 Z. Zou, J. Ye, K. Sayama and H. Arakawa, *Nature*, 2001, **414**, 625–627.
116 Z. Zou and H. Arakawa, *J. Photochem. Photobiol., A*, 2003, **158**, 145–162.
117 M. Douiheche, R. Haberkorn and H. P. Beck, *Z. Naturforsch., B: J. Chem. Sci.*, 2008, **63**, 1160–1168.
118 A. C. Malingowski, P. W. Stephens, A. Huq, Q. Huang, S. Khalid and P. G. Khalifah, *Inorg. Chem.*, 2012, **51**, 6096–6103.
119 K. Maeda, T. Takata, M. Hara, N. Saito, Y. Inoue, H. Kobayashi and K. Domen, *J. Am. Chem. Soc.*, 2005, **127**, 8286–8287.
120 M. Yoshida, K. Takanabe, K. Maeda, A. Ishikawa, J. Kubota, Y. Sakata, Y. Ikezawa and K. Domen, *J. Phys. Chem. C*, 2009, **113**, 10151–10157.
121 K. Maeda, K. Teramura, H. Masuda, T. Takata, N. Saito, Y. Inoue and K. Domen, *J. Phys. Chem. B*, 2006, **110**, 13107–13112.
122 K. Maeda, K. Teramura and K. Domen, *J. Catal.*, 2008, **254**, 198–204.
123 K. Maeda, A. Xiong, T. Yoshinaga, T. Ikeda, N. Sakamoto, T. Hisatomi, M. Takashima, D. Lu, M. Kanehara, T. Setoyama, T. Teranishi and K. Domen, *Angew. Chem., Int. Ed.*, 2010, **49**, 4096–4099.
124 Y. Lee, H. Terashima, Y. Shimodaira, K. Teramura, M. Hara, H. Kobayashi, K. Domen and M. Yashima, *J. Phys. Chem. C*, 2007, **111**, 1042–1048.
125 Y. Lee, K. Teramura, M. Hara and K. Domen, *Chem. Mater.*, 2007, **19**, 2120–2127.
126 X. Wang, K. Maeda, Y. Lee and K. Domen, *Chem. Phys. Lett.*, 2008, **457**, 134–136.
127 S. Mubeen, J. Lee, N. Singh, S. Krämer, G. D. Stucky and M. Moskovits, *Nat. Nanotechnol.*, 2013, **8**, 247–251.
128 K. Maeda, D. Lu and K. Domen, *Chem. – Eur. J.*, 2013, **19**, 4986–4991.
129 C. Liu, J. Tang, H. M. Chen, B. Liu and P. Yang, *Nano Lett.*, 2013, **13**, 2989–2992.
130 R. Asai, H. Nemoto, Q. Jia, K. Saito, A. Iwase and A. Kudo, *Chem. Commun.*, 2014, **50**, 2543–2546.
131 L. Liao, Q. Zhang, Z. Su, Z. Zhao, Y. Wang, Y. Li, X. Lu, D. Wei, G. Feng, Q. Yu, X. Cai, J. Zhao, Z. Ren, H. Fang, F. Robles-Hernandez, S. Baldelli and J. Bao, *Nat. Nanotechnol.*, 2014, **9**, 69–73.
132 J. Liu, Y. Liu, N. Liu, Y. Han, X. Zhang, H. Huang, Y. Lifshitz, S.-T. Lee, J. Zhong and Z. Kang, *Science*, 2015, **347**, 970–974.
133 C. Pan, T. Takata, M. Nakabayashi, T. Matsumoto, N. Shibata, Y. Ikuhara and K. Domen, *Angew. Chem., Int. Ed.*, 2015, **54**, 2955–2959.
134 J. Xu, C. Pan, T. Takata and K. Domen, *Chem. Commun.*, 2015, **51**, 7191–7194.
135 Y. Sasaki, H. Nemoto, K. Saito and A. Kudo, *J. Phys. Chem. C*, 2009, **113**, 17536–17542.
136 Q. Jia, A. Iwase and A. Kudo, *Chem. Sci.*, 2014, **5**, 1513–1519.
137 A. Iwase, Y. H. Ng, Y. Ishiguro, A. Kudo and R. Amal, *J. Am. Chem. Soc.*, 2011, **133**, 11054–11057.
138 S. S. K. Ma, K. Maeda, T. Hisatomi, M. Tabata, A. Kudo and K. Domen, *Chem. – Eur. J.*, 2013, **19**, 7480–7486.
139 Q. Wang, T. Hisatomi, S. S. K. Ma, Y. Li and K. Domen, *Chem. Mater.*, 2014, **26**, 4144–4150.
140 R. Kobayashi, S. Tanigawa, T. Takashima, B. Ohtani and H. Irie, *J. Phys. Chem. C*, 2014, **118**, 22450–22456.
141 T. F. Yeh, C. Y. Teng, S. J. Chen and H. Teng, *Adv. Mater.*, 2014, **26**, 3297–3303.
142 A. J. Nozik, *Appl. Phys. Lett.*, 1977, **30**, 567–569.
143 K. Sayama, K. Mukasa, R. Abe, Y. Abe and H. Arakawa, *Chem. Commun.*, 2001, 2416–2417.
144 Y. Sasaki, H. Kato and A. Kudo, *J. Am. Chem. Soc.*, 2013, **135**, 5441–5449.
145 C. A. Linkous, D. K. Slattery, *Proc. 2000 Hydrog. Progr. Rev.* 2000, *NREL/CP-570*-28890, 1–13.
146 S. Ardo and G. J. Meyer, *Chem. Soc. Rev.*, 2009, **38**, 115–164.
147 B. H. Farnum, J. M. Gardner and G. J. Meyer, *Inorg. Chem.*, 2010, **49**, 10223–10225.
148 K. Sayama, K. Mukasa, R. Abe, Y. Abe and H. Arakawa, *J. Photochem. Photobiol., A*, 2002, **148**, 71–77.

149 Y. Miseki, S. Fujiyoshi, T. Gunji and K. Sayama, *Catal. Sci. Technol.*, 2013, **3**, 1750–1756.
150 Y. Miseki, H. Kusama, H. Sugihara and K. Sayama, *J. Phys. Chem. Lett.*, 2010, **1**, 1196–1200.
151 R. Abe, T. Takata, H. Sugihara and K. Domen, *Chem. Commun.*, 2005, 3829–3831.
152 M. Higashi, R. Abe, K. Teramura, T. Takata, B. Ohtani and K. Domen, *Chem. Phys. Lett.*, 2008, **452**, 120–123.
153 K. Maeda, M. Higashi, D. Lu, R. Abe and K. Domen, *J. Am. Chem. Soc.*, 2010, **132**, 5858–5868.
154 K. Maeda, *ACS Appl. Mater. Interfaces*, 2014, **6**, 2167–2173.
155 M. Higashi, R. Abe, A. Ishikawa, T. Takata, B. Ohtani and K. Domen, *Chem. Lett.*, 2008, **37**, 138–139.
156 M. Tabata, K. Maeda, M. Higashi, D. Lu, T. Takata, R. Abe and K. Domen, *Langmuir*, 2010, **26**, 9161–9165.
157 J. Kiwi and M. Grätzel, *Angew. Chem., Int. Ed. Engl.*, 1979, **18**, 624–626.
158 J. Kiwi, E. Borgarello, E. Pelizzetti, M. Visca and M. Grätzel, *Angew. Chem., Int. Ed. Engl.*, 1980, **19**, 646–648.
159 C. A. Linkous, *DOE Contract Number DE-FC36-95G0100062*, 1999, 1–153.
160 G. Munuera, V. Rives-Arnau and A. Saucedo, *J. Chem. Soc., Faraday Trans. 1*, 1979, **75**, 736–747.
161 E. Borgarello, J. Kiwi, M. Grätzel, E. Pelizzetti and M. Visca, *J. Am. Chem. Soc.*, 1982, **104**, 2996–3002.
162 A. Mills and S. Le Hunte, *J. Photochem. Photobiol., A*, 1997, **108**, 1–35.
163 R. Abe, K. Shinmei, K. Hara and B. Ohtani, *Chem. Commun.*, 2009, 3577–3579.
164 R. Abe, K. Shinmei, N. Koumura, K. Hara and B. Ohtani, *J. Am. Chem. Soc.*, 2013, **135**, 16872–16884.
165 Y. Sasaki, A. Iwase, H. Kato and A. Kudo, *J. Catal.*, 2008, **259**, 133–137.
166 H. Kato, Y. Sasaki, N. Shirakura and A. Kudo, *J. Mater. Chem. A*, 2013, **1**, 12327–12333.
167 R. Niishiro, S. Tanaka and A. Kudo, *Appl. Catal., B*, 2014, **150–151**, 187–196.
168 W. Wang, J. Chen, C. Li and W. Tian, *Nat. Commun.*, 2014, **5**, 4647.
169 M. Kato, T. Cardona, A. W. Rutherford and E. Reisner, *J. Am. Chem. Soc.*, 2012, **134**, 8332–8335.
170 C. M. Elliott, S. Caramori and C. A. Bignozzi, *Langmuir*, 2005, **21**, 3022–3027.
171 S. Mathew, A. Yella, P. Gao, R. Humphry-Baker, B. F. E. Curchod, N. Ashari-Astani, I. Tavernelli, U. Rothlisberger, M. K. Nazeeruddin and M. Grätzel, *Nat. Chem.*, 2014, **6**, 242–247.
172 M. A. Green, K. Emery, Y. Hishikawa, W. Warta and E. D. Dunlop, *Prog. Photovolt.: Res. Appl.*, 2015, **23**, 1–9.

